

DIRECTOR'S COPY



Axisymmetric Infiltration

by

Royal H. Brooks

Paul J. Leclercq

Richard R. Tebbs

Walter Rawls

Paul H. River Health Comm.
LIBRARY
P. O. Box 906 - Vancouver, Wa. 98660
(206) 681-2661 (503) 285-3400




Water Resources Research Institute

Oregon State University

Corvallis, Oregon

WRRI-22

January 1974





Axisymmetric Infiltration

by

Royal H. Brooks
Paul J. Leclercq
Richard R. Tebbs
Walter Rawls

Final Report

Submitted to

The Offices of Water Resources Research

Oregon State University
Corvallis, Oregon

January 1974

PREFACE

The work reported herein was performed under the annual allotment from the Office of Water Resources Research to the Oregon Water Resources Research Institute. Funds were available over a three year period, but due to difficulty in acquiring graduate students, the total time spent on the project was only 21 months.

The second author on the report was supported in the Department of Agricultural Engineering as a research assistant and completed a Master's Degree in June of 1973. All of the experimental work reported herein was performed by him during his graduate study.

The project has truly been a cooperative effort from the very beginning to its conclusion. The objectives of the project were formulated after a series of meetings between the Northwest Watershed Research Center of the Agricultural Research Service in Boise, Idaho and the Department of Agricultural Engineering at Oregon State University.

The development of the mathematical model and programming were performed by a staff member from the Southern Utah State College in Cedar City, Utah during time spent at Oregon State University working toward a Ph.D. in mathematics.

The work reported herein is preliminary and considerable additional work is needed to bring the project to a firm conclusion. Some of the results, therefore, are not conclusive and should be considered tentative and should be used with discretion.

The project will be pursued on a much larger scale under a new grant from the Office of Water Resources Research.

Hopefully, this report will lead engineers and scientists closer to more accurate predictive models concerning the management of watersheds, the engineering design of hydraulic structures, and the forecasting of water supplies.

Axisymmetric Infiltration

by

Royal H. Brooks¹, Paul J. Leclercq², Richard R. Tebbs³, and Walter Rawls⁴

INTRODUCTION

Engineers concerned with watershed protection and flood control and other engineering problems associated with watershed hydrology are often confronted with predicting watershed characteristics. Watershed models or empirical equations are often used to make these predictions.

Almost all predictive schemes or models for determining runoff, the development of stream hydrographs, and other watershed characteristics require some historical performance data for fitting to the model. Where these data are available, these predictive models are useful for extrapolating the watershed characteristics to future times and events.

However, the prediction of watershed characteristics for ungaged watersheds requires the use of empirical equations that are often not physically meaningful or do not include meaningful physical data from the watershed. Such data as area of watershed, type of vegetative cover, etc. are not very meaningful when it comes to predicting infiltration and runoff. Recently there have been some attempts to construct physically based watershed models that include the various physical processes that take place on the watershed during a rainfall event. The infiltration process is one of the

¹Associate Professor, Department of Agricultural Engineering, Oregon State University, Corvallis, Oregon.

²Hydrologist, Faculte des Sciences Agronomiques, Department de Genie Rural, Universito Catholique de Louvain, Belgium.

³Assistant Professor, Department of Mathematics, Southern Utah State College, Cedar City, Utah.

⁴Hydrologist, Northwest Watershed Research Center, Western Region, Agricultural Research Service, USDA, Boise, Idaho.

more important components of the rainfall-runoff process that has recently received some attention by Mein and Larson (1973), Jeppson (1972), and Singh (1972).

These authors have constructed an infiltration model based upon the partial differential equation describing the movement of water through soils. The use of this model requires information concerning the relationships among permeability, capillary pressure, and soil-water content.

In all likelihood, these deterministic models will have limited use in the solution of watershed systems, particularly if the watersheds are large and diverse. Capillary pressure, permeability, and soil-water content relationships are usually obtained for relatively small samples of soil that only represent points in the total watershed. The relationship among these variables may be greatly different with respect to depth in the profile and with respect to aerial distribution over the watershed. Nevertheless, these models are very useful for learning how the properties of the soil affect the infiltration process.

Unless an effort is made to generalize the functional relationship in the solution of the infiltration model, little may be gained by using specific data of capillary pressure, permeability, and water content in the model. One can only ascertain how a particular soil affects the processes. It would be much more helpful to know how broad classes of soil texture and layering affect the infiltration process so that the watershed may be broken down into characteristic units. The problem arises in making broad classifications that are quantitative.

The work on similitude in porous media by Brooks and Corey (1964) may be of some use in making broad descriptive classifications of soils that are quantitative and at the same time useful in solutions of models.

The purpose of this report is to show how the hydraulic properties of porous media affect infiltration where infiltration is defined as the entry of water into the soil from a source at the soil surface and the subsequent movement of the water through the soil. Specifically, it includes infiltration rate and advance of the wetting front. The hydraulic properties of porous media described by Brooks and Corey (1964, 1966) are used to describe the infiltration process.

These hydraulic properties are obtained and defined from the capillary pressure-saturation curves for drainage. Since the infiltration of water into soil is an imbibition process, these hydraulic properties must be related to capillary pressure and saturation for imbibition. These capillary pressure-saturation curves for imbibition and drainage are different because of the entrapment of air. The phenomena is called hysteresis.

This report describes in detail a rapid method for measuring capillary pressure saturation curves for both imbibition and drainage. A functional relationship between capillary pressure and saturation for imbibition is proposed that includes the properties obtained from the drainage capillary pressure-saturation curve.

Finally, the infiltration under a circular infiltrometer is computed from a mathematical model and compared with experimental data. The solutions were obtained using both imbibition and drainage functions. The solutions are presented in terms of scaled variables to show the effect of hydraulic properties upon infiltration rate and advance of the wetting front.

SIMILITUDE CRITERIA AND THE MODEL FOR FLUID FLOW IN POROUS MEDIA

Whenever a model is constructed to represent a flow system, it is important that the model behaves in a manner similar to the prototype. The model presented herein is a mathematical model that describes the flow of a liquid in porous media. It does not resemble the prototype in physical appearance as opposed to a physical model that would be a miniature of the prototype.

If one were to construct a physical model for observing fluid flow in porous media it would become obvious that the model must be constructed so that its dimensions were similar or proportional to the prototype, and that it should behave in a similar manner. Yet very often when mathematical models are constructed for this purpose, little or no attention is given to similarity so that its performance can be extended to similar prototypes.

Obviously, the number of solutions from a mathematical model can be infinite because there are an infinite set of boundary conditions that may be imposed. Each set of conditions yields different sets of outputs or solutions.

The literature is replet with the solution of various boundary value problems that have application only to one prototype situation. Some of these solutions were obtained with mathematical models while others were obtained using physical models. Extrapolation or the extension of results to other similar situations are virtually impossible because the solutions have not been presented in terms of scaled variables or scaled boundaries that satisfy similarity criteria.

By satisfying similarity criteria one not only may extend the results to a similar prototype, but generalizations can be made that provide an

insight into the physical nature of how the system performs. Without similarity criteria it becomes difficult to make generalized conclusions.

There are two generally accepted methods for establishing criteria of similitude. The first is usually called dimensional analysis that is commonly used by hydraulic engineers. The second method is called inspectional analysis and requires that the differential equation describing the physical processes is known.

The purpose of this section is not to review or discuss the various methods of establishing similitude requirements, but rather to apply criteria to the flow of fluids in porous media that has been formerly developed.

The similitude requirements proposed by Brooks and Corey (1964) will be reviewed and applied to the mathematical model described herein. They found that by applying the method of inspectional analysis to the general flow equation of one fluid moving in a homogeneous media a set of requirements could be established. They discovered that if these requirements were satisfied, the solutions of the differential equations yielded identical particular solutions in terms of scaled variables.

The basic model used for the flow of fluids in porous media is obtained by combining Darcy's Law with the continuity equation. The basic units in this equation are force, length, and time. The properties of the fluid and the media can be defined in terms of these three basic units. For example, permeability can be expressed in terms of length.

If the basic equation is written in terms of energy per unit volume, then the equation may be appropriately scaled by using a standard unit of energy that contains standard units of force and length. Since permeability may be a variable, then a standard unit of permeability must be chosen also.

The basic flow equation, Darcy's Law may be expressed as

$$q = -K_e \nabla (-P_c/\rho g + Z) \quad (1)$$

or in terms of energy per unit volume, it becomes

$$q = -\frac{k_e}{\mu} \nabla (-P_c + \rho g Z). \quad (2)$$

A standard unit of pressure and permeability are chosen, i.e., P_o and K_o respectively. The physical significance of these terms will be pointed out later in the development. By dividing each pressure term by the standard pressure and permeability by the standard permeability, the standard units for the other terms in the equation may be deduced. After following this scaling procedure, equation (2) becomes

$$q/K_o = \frac{k_e P_o}{K_o \mu} \nabla (-P_c/P_o + \rho g Z/P_o). \quad (3)$$

Since $k_e = \frac{K\mu}{\rho g}$, then equation (3) may be expressed as

$$q/K_o = \frac{K}{K_o} \frac{(P_o)}{(\rho g)} \nabla \left(-\frac{P_c}{P_o} + \frac{\rho g Z}{P_o} \right). \quad (4)$$

The standard unit of length for the gradient, ∇ , must be $P_o/\rho g$ and the standard flux, q , must be K_o .

Using simplified notation and rewriting equation (4) the expression

$$q. = K.\nabla.(-P. + Z.) \quad (5)$$

is obtained which is identical in form to equation (1). The dot notation is defined as

$q.$ = scaled flux, q/k_o ,

$\nabla.$ = scaled gradient, $L_o \nabla$,

$P.$ = scaled pressure, P_c/P_o ,

$Z.$ = scaled elevation above an arbitrary datum, Z/L_o , and L_o is the standard length or $L_o = P_o/\rho g$.

Obviously, if one chooses a standard pressure, the standard unit of energy and the characteristic length for similitude must be $P_o/\rho g$ or some particular characteristic pressure head.

For saturated media, K_o is a constant and the standard pressure head $P_o/\rho g$ may be any characteristic pressure head related to the flow geometry or any characteristic length. The properties of the medium do not become part of the similitude criteria. As long as the medium is always saturated, the only similitude criteria that must be satisfied are those for geometric similarity, i.e.,

1. The macroscopic boundaries of the model must have a shape and orientation similar to the prototype.
2. The size of the model must be such that the ratio of all corresponding lengths must be the same for model and prototype, i.e.,

$$\left(\frac{L}{D}\right)_m = \left(\frac{L}{D}\right)_p \quad (6)$$

If at any time in the flow system, the medium becomes partially saturated so that

$$K. = f(P.) \quad (7)$$

then a geometric characteristic length is not sufficient for use as a standard pressure head or as a standard length. In other words, for the general

case, the standard pressure head and standard permeability cannot be arbitrarily chosen. If the relative flux, q ., in equation (5) must be the same for both prototype and model, the functional relationship given by equation (7) must be identical for both model and prototype.

Even though the relationship given by equation (7) is different for wetting and drying of media, the standard units used in equation (7) should be intrinsic media properties and independent of the type of flow. If the standard units for similarity are to be practical, they should be measurable also.

In studies dealing with the drainage of liquids from porous media, Brooks and Corey (1964) found that effective saturation and capillary pressure could be related by the power function

$$S. = (P.)^{-\lambda} \text{ for } P. \geq 1.0, \tag{8}$$

and

$$S. = 1.0 \text{ for } P. \leq 1.0$$

where $P. = P_c/P_b$ and $S. = (S - S_r)/(1 - S_r)$. They showed that permeability as a function of capillary pressure and saturation may be deduced from equation (8) through the Burdine Integral. The relationship is a power function also and may be expressed as

$$K. = (P.)^{-(2 + 3\lambda)} \text{ for } P. \geq 1.0,$$

$$K. = 1.0 \text{ for } P. \leq 1.0, \text{ where } K. = K_e/K_s, \tag{9}$$

and

$$K. = (S_e)^{2/\lambda + 3}$$

It should be obvious that if this functional form is valid for drainage, the bubbling pressure head P_b and the saturated permeability K_s reduce the functional relationship among the variables to one that is the same for all soils having identical values of λ . Therefore, these two hydraulic properties of porous media logically become the standard pressure and permeability for satisfying the general similitude requirements for flow in porous media. The requirements necessary and sufficient for two systems to be similar in addition to those already expressed for geometric similarity, is that the pore size distribution index, λ , must be the same and the characteristic or standard length must be the bubbling pressure head. In other words, the size of the model must be such that

$$\frac{L_p}{L_m} = \frac{(P_b/\rho g)_p}{(P_b/\rho g)_m}$$

and

(10)

$$\lambda_m = \lambda_p,$$

where L is any characteristic length. Corey, et.al, (1965) demonstrated that if the above similitude requirements were satisfied for the drainage cycle, the two systems would be similar on the imbibition cycle as well. Their study, however was limited to sand separates and was by no means conclusive. In fact, their functional relationship for imbibition was the same as that used for drainage. No imbibition experiments, however, were run to test the similitude criteria for imbibition. It is more than likely that the above requirements for similitude are minimal and that for imbibition additional criteria may be required.

The general scaled differential equation for imbibition or drainage is obtained by combining scaled Darcy's Law with the scaled continuity equation.

The continuity equation is scaled in a manner similar to Darcy's Law and in dimensional form it may be written as

$$\operatorname{div} \left(\frac{q}{\phi_e} \right) = - \frac{\partial S.}{\partial t} \quad (11)$$

where ϕ_e is effective porosity.

If q is scaled by K_s , t by t_o , and $\operatorname{div.}$ by $P_b/\rho g$, then equation (11) becomes

$$\left(\frac{t_o K_s}{\phi_e P_b / \rho g} \right) \left(\frac{P_b}{\rho g} \right) \operatorname{div} \left(\frac{q}{K_s} \right) = - \frac{\partial S.}{\partial t / t_o} \quad (12)$$

or

$$\left(\frac{t_o K_s}{\phi_e P_b / \rho g} \right) (\operatorname{Div.} q.) = - \frac{\partial S.}{\partial t.} \quad (13)$$

Since equation (13) must be identical in form to equation (11) and must yield identical particular solutions, let

$$\frac{t_o K_s \rho g}{\phi_e P_b} = 1 \quad (14)$$

or

$$t_o = \frac{P_b \phi_e}{\rho g K_s} \quad (15)$$

Thus, for unsteady flow in porous media, the standard time is given by equation (15) and the general scaled equation for flow of one fluid in partially saturated media becomes

$$\text{DIV.}\{K.\nabla.(-P. + Z.)\} = \partial S./\partial t. \quad (16)$$

where the dots designate scaled variables or operators with respect to scaled variables.

The scaled partial differential equation (16) may be rearranged in terms of other dependent variables, eg., scaled saturation, $S.$, or scaled hydraulic head, $H.$ When equation (16) is written in terms of a particular set of coordinates for a given set of boundary and initial conditions, it becomes a model for fluid movement in porous media.

Equation (16) may be solved using any suitable relationship among saturation, capillary pressure, and permeability provided these variables are scaled with the standard quantities previously mentioned. If the pore size distribution index is known, then the results will have application to other similar boundary conditions having the same pore size distribution index. The relationships among the variables, saturation, capillary pressure, and permeability, need not be in functional form. They may be in terms of a set of corresponding values (tabular) and they may be for either imbibition, drainage, or for flow situations where hysteresis is present.

The standard units of permeability, capillary pressure, and saturation are intrinsic properties of the media and one need not be concerned with the type of function (or tabular data) used to describe the flow process so long as the media properties described by Brooks and Corey are definable. If they cannot be defined, then the solutions are not transferable to other similar conditions.

A summary of the standard units used in equation (16) and other hydraulic properties of media, are given in Table 1 below. Other standard units may be defined from those given in Table 1, eg., diffusivity and hydraulic head.

Table 1. Standard Units and Hydraulic Properties of Media.

Length	$L_o = P_b / \rho g$
Time	$t_o = P_b \phi_e / \rho g K_s$
Permeability	$K_o = K_s$
Water content, volumetric	$\theta_o = \phi_e$
Effective saturation	$\theta / \theta_o = S.$
Capillary pressure	$P_o = P_b$
Pore size distribution index	λ
Effective porosity	$\phi_e = \phi(1-S_r)$
Residual saturation	S_r

HYDRAULIC PROPERTIES OF MEDIA AND IMBIBITION

True similitude requirements for flow of fluids in partially saturated media should be independent of the character of the flow, previous history of the media, and type of boundary conditions. Since infiltration or imbibition is largely dependent upon the phenomena capillarity, a brief discussion of capillarity with emphasis on imbibition follows.

When water enters a soil, air must be replaced. The flow process, therefore, involves two immiscible fluids, air and water. When these two immiscible fluids occupy the same pore volume of a porous medium, water is

more strongly adsorbed than air, creating a curved interface between the two fluids. In other words, the cohesive forces in the water are weaker than the adsorptive forces. This strong adsorption of the water to the solid creates a curved interface such that the pressure is decreased in the water or on the convex side of the interface relative to that on the concave side. The smaller the space for these two fluids to occupy, the smaller the radius of curvature of the interface and the greater the pressure difference across the interface. This pressure difference is called capillary pressure and is defined by the equation

$$P_c = P_a - P_w \quad (17)$$

where the subscripts refer to air and water. Since capillary pressure can be related also to the radius of curvature of the interface, the basic equation of capillarity given in general terms is

$$P_c = \sigma \left(\frac{1}{r_1} + \frac{1}{r_2} \right) \quad (18)$$

where r_1 and r_2 are the major and minor radii of curvature and σ is the surface tension of the wetting fluid.

In the work described herein, the air is assumed to be at atmospheric pressure and further, no resistance is encountered in its flow. Therefore, the permeabilities discussed will be water permeabilities and saturations (fraction of pore volume occupied by a fluid) will refer to the water phase.

Large values of capillary pressure produce small radii of curvature according to equation (2) and hence, low values of saturation. In other words, saturation depends upon capillary pressure.

The direction of saturation change is used to describe the character of fluid flow in porous media. An increase in saturation is designated "imbibition" while a decrease in saturation is called "drainage".

The functional relationship between saturation and capillary pressure depends upon the character of flow and the initial and residual saturation of the soil at the beginning or end of the imbibition or drainage cycle. This phenomena is called hysteresis.

According to Colonna, et.al. (1972), during drainage, the air begins to penetrate progressively into pores having smaller and smaller sizes. For each increment of capillary pressure increase, there is activated a new family of pore networks consisting of interconnected pores of varying sizes that are equal or larger than the ones already penetrated by air.

The activation of each new network of pores is controlled by the capillary pressure necessary to allow air first to penetrate and then to flow through the channels that belong to the network. Colonna, et.al., referred to this capillary pressure as the "opening pressure".

For imbibition, the capillary pressure necessary to repenetrate each of these networks to prevent air flow is called the "stoppage pressure." It could, in theory, be as high as the bubbling pressure of media having completely uniform pore sizes.

During imbibition, part of the air is bypassed by the increasing water saturation leaving a portion of the air trapped in the media. This air trapped in the media at a particular capillary pressure prevents water from filling the pores to the saturation obtainable under "drainage". Therefore, if two identical media are at the same capillary pressure but one is on the imbibition cycle and the other on the drainage cycle, the saturation

and permeability will be smaller for the imbibing media than for the one draining.

It is well known that drainage and imbibition capillary pressure-saturation curves can be perfectly reproduced provided the saturation is always reduced to a value near residual on the drainage cycle and to near zero on the imbibition cycle. Therefore, under these specified end points each cycle has a unique functional relationship among capillary pressure, saturation, and permeability to both air and water.

Since the hydraulic behavior of fluids in porous media is largely affected by capillary pressure and its relation to saturation and permeability, it would be useful to characterize the infiltration process with capillary properties of the soil.

The hydraulic properties of porous media defined by Brooks and Corey (1964) from drainage curves for describing similitude requirements will be employed here to study infiltration. This will be accomplished by defining the capillary pressure-saturation curves for imbibition in terms of the hydraulic properties of the drainage curve.

In order to accomplish this, it is necessary to have capillary pressure-saturation data for many soils for both imbibition and drainage. Since there is not an abundance of data in the literature where both imbibition and drainage are obtained on the same soils, one must resort to measuring capillary pressure as a function of saturation and permeability. The process of acquiring data for a large number of soils by conventional techniques is very time consuming. Therefore, a considerable part of the research effort was devoted to developing an experimental technique for rapidly determining capillary pressure as a function of saturation for both imbibition and drainage.

Experimental Technique for Determining Hydraulic Properties

Most experimental procedures for determining capillary pressure as a function of saturation impose a positive air pressure on a soil sample in contact with a fully saturated capillary barrier or a negative pressure is applied to the fluid on the opposite side of the fully saturated barrier. In both cases, when the pressure changes, liquid either leaves or enters the soil through the capillary barrier.

The liquid content in the soil sample will change continuously until the capillary forces in the soil come into equilibrium with the forces imposed on the sample or on the capillary barrier. The time required for equilibrium is considerable.

In general, the method described herein for measuring imbibition capillary pressure-saturation is one in which no liquid enters the soil through the capillary barrier. Liquid is applied to the soil sample in equal increments through the use of a micrometer pipette. When liquid is added, the capillary pressure in the soil sample is reduced and the equilibrium pressure is measured on the opposite side of a fully saturated capillary barrier. The details of the method are described in Appendix I.

Experimental Data

Some typical data obtained by the method described in Appendix I is shown in Figure 1. The data is expressed in terms of scaled variables and the hydraulic properties are shown in the figure. The imbibition curve is scaled using the bubbling pressure and residual saturation from the drainage curve. The solid lines passing through the drainage points make up the curve computed from equation 8.

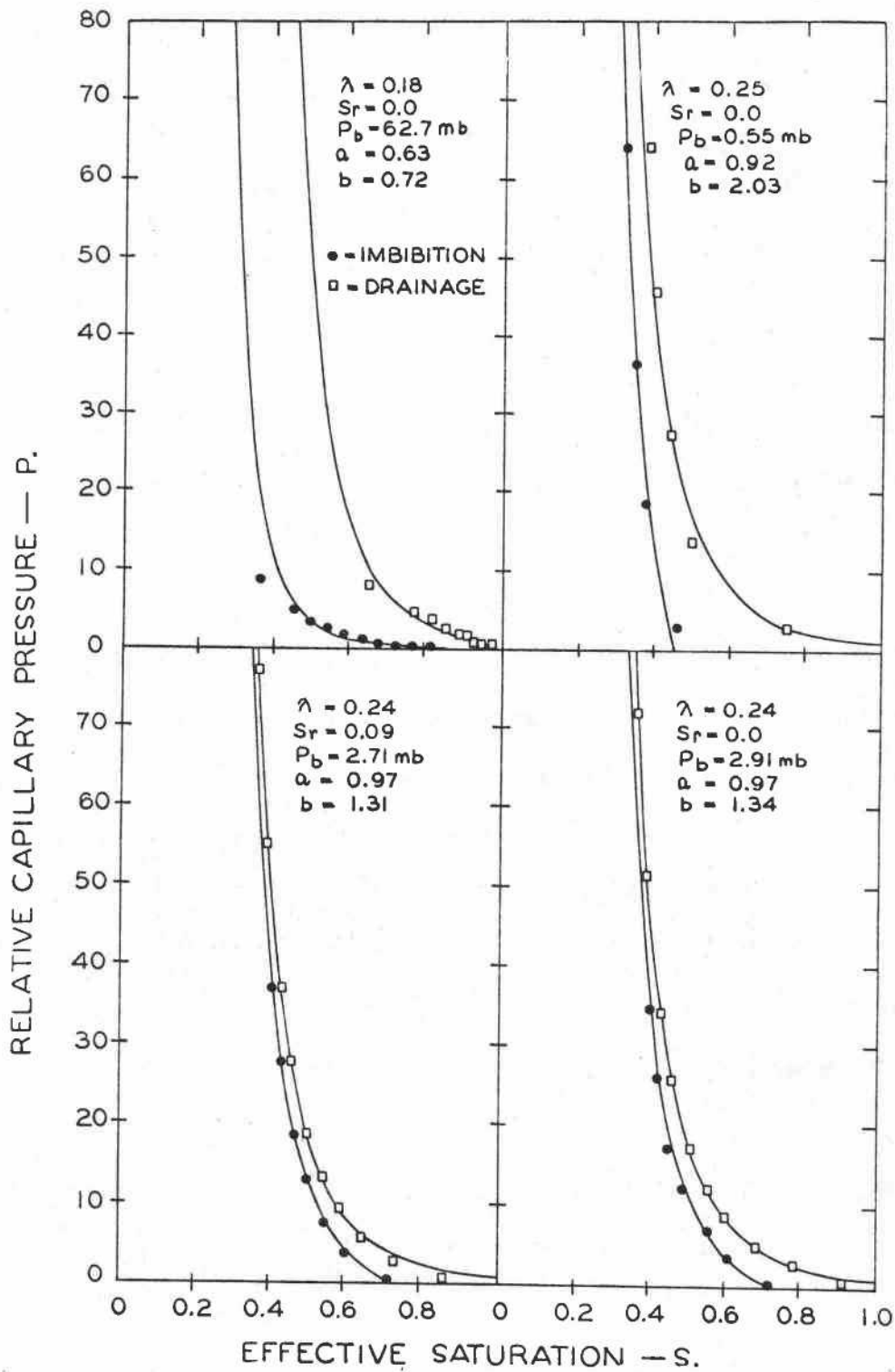


Figure 1. Relative capillary pressure as a function of effective saturation obtained from soil cores for imbibition and drainage compared with theoretical equations.

The imbibition data for these media were fitted to the expression

$$S_e = \frac{a}{(p. + b^{1/\lambda})^\lambda} \quad (19)$$

where a and b are arbitrary constants, $P.$ is scaled capillary pressure and λ is the pore size distribution index from equation 8 for the drainage data. The value of residual saturation, S_r , contained in the definition of S_e is the value obtained from the drainage data also. The ratio of a/b is the value of effective saturation when the capillary pressure is zero.

No physical significance is attached to the parameters a and b at this stage of development, for obtaining a general expression for effective saturation as a function of capillary pressure. Furthermore, their value must be determined from experimental imbibition data. It is highly desirable to determine these parameters (or any others used in an imbibition expression) from the drainage data, thereby permitting the imbibition function to be calculated from drainage data.

The solid lines passing through the imbibition data in Figure 1 were computed from equation (19). The fit of both theoretical curves to the imbibition and drainage data seems reasonable and sufficiently accurate for purposes of studying infiltration.

Equation (19) becomes part of the infiltration model since a functional relationship among saturation, capillary pressure, and permeability is required for the solution of equation (16), which is the basic form of the infiltration model discussed herein.

A relationship between saturation and permeability is the only remaining part of the model that needs to be constructed. Brooks and Corey

(1964) derived a relationship from equation (8) for the drainage case by using the Burdine integral.

Some effort has been made during this study to deduce a permeability relationship from equation (19) but without success. In the absence of this relationship, a form of the Brooks-Corey permeability equation given by

$$K_r = \frac{a}{b}(S_e)^{2/\lambda + 3} \quad (20)$$

will be used in order to complete the infiltration model. One would not expect the imbibition function of permeability-saturation to be greatly different from the drainage function.

It has been observed experimentally that many sands when allowed to imbibe water to reduce the capillary pressure to zero have permeabilities near 50 percent of their saturated value. The corresponding saturation is usually 0.85. Using a value of 2.0 for λ and 0.85 for S_e , the relative permeability from equation 18 is 0.52. It will be necessary to obtain additional experimental data on imbibition permeability before a more exact expression can be derived.

No physical interpretation is attached to the parameters a and b in equation (19) and (20). However, if two media are to be similar, their functional relationships among capillary pressure, saturation, and permeability must be the same for both and two additional similitude requirements are needed for infiltration.

The effect of the parameters a and b upon the capillary pressure-saturation curve is shown in Figures 2 and 3. Larger values of a and b tend to steepen the curves for small values of λ . For large values of λ ,

Figure 2. Theoretical curves of relative capillary pressure as a function of effective saturation for various values of λ and for $a = b = 1.5$.

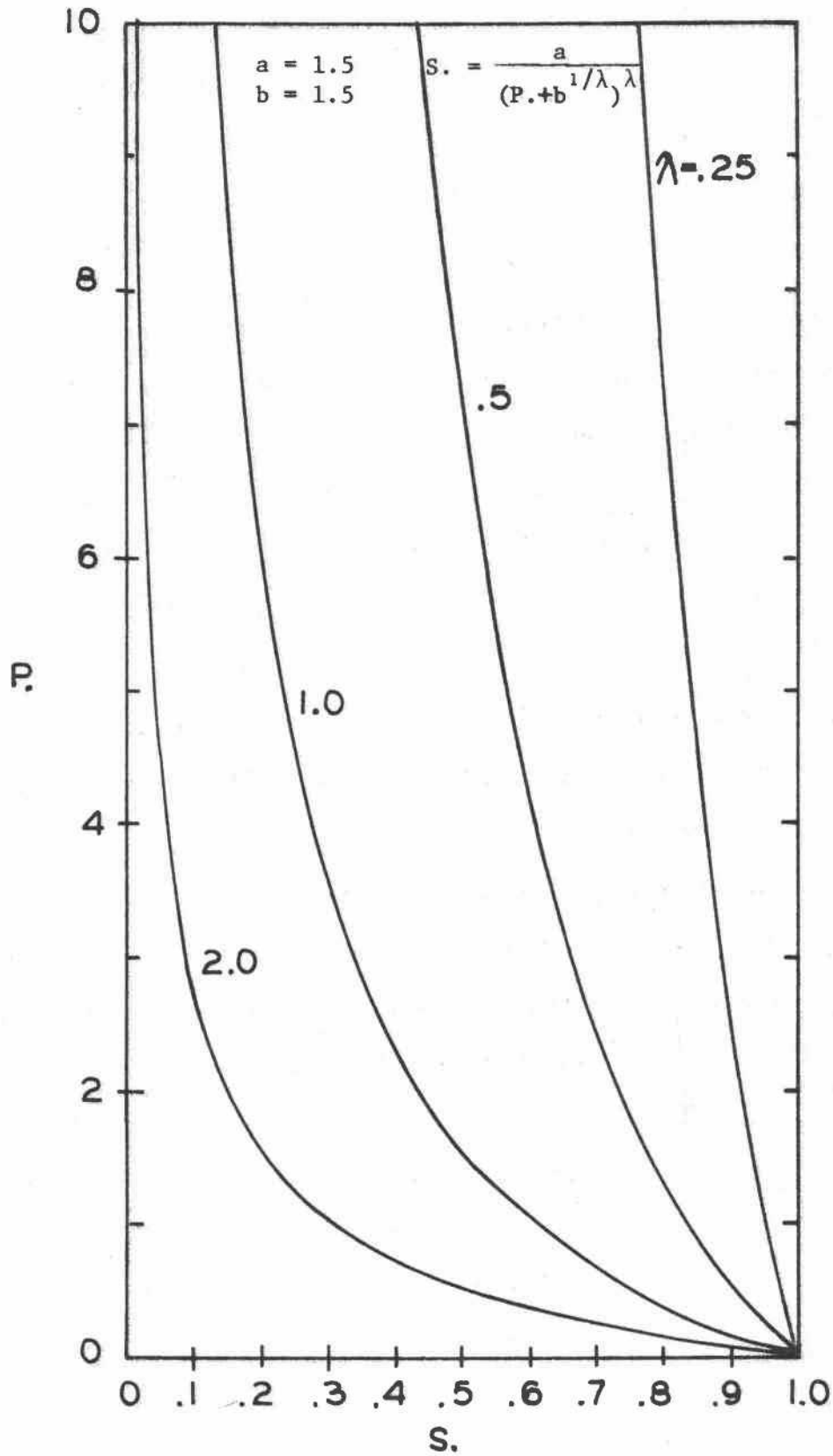
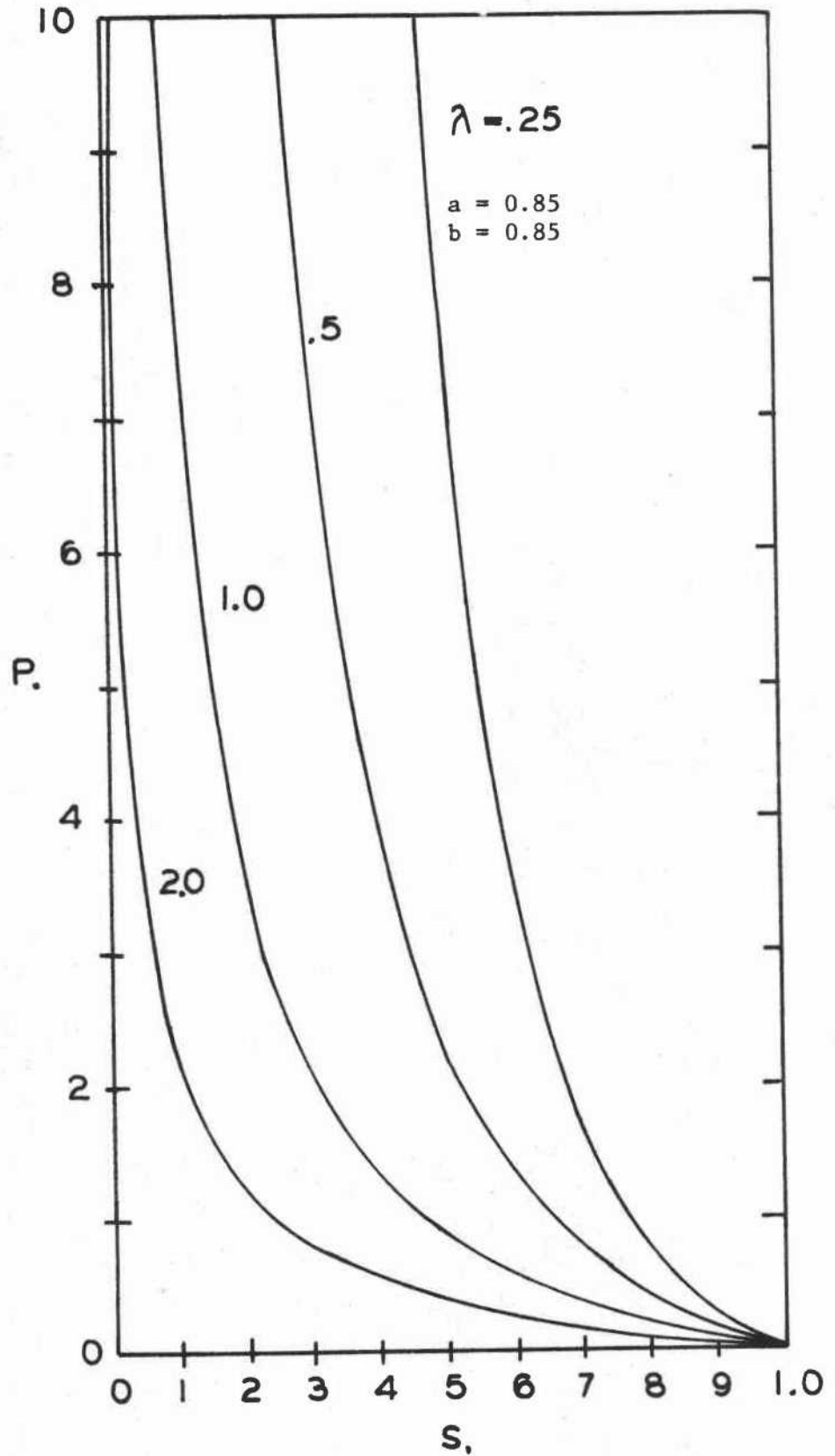


Figure 3. Theoretical curves of relative capillary pressure as a function of effective saturation for various values of λ and for $a = b = 0.85$.

$$S_r = \frac{a}{(P_c + b^{1/\lambda})^\lambda}$$



the value of a and b have little effect. The imbibition function, equation (19), is different from the drainage function of Brooks and Corey in that there is no range of capillary pressure where saturation is invariant.

Laboratory data have been obtained from soil samples where saturation has been invariant with capillary pressure on the imbibition cycle. Equations (19) and (20) will probably not be adequate for such soils.

THEORETICAL INFILTROMETER

Infiltration of water into a homogeneous layer of soil from a circular source placed at the soil surface will be examined by constructing a mathematical model from equation (16). The distribution of water in the soil, the shape of the wetting front and the infiltration capacity curve may be obtained from the model.

Consider a soil profile of depth, D, at a uniform initial saturation. The lower boundary is impermeable. The upper boundary is defined in two parts; (1) within the radius of the infiltrometer where the capillary pressure equals zero and (2) beyond the radius of infiltration where the flow across the boundary is negligible. Because the infiltration source is circular, two other boundaries are created. The line perpendicular to the soil surface and through the center of the circle is a mathematical line of symmetry, hence the flow across it is zero. The other is the axisymmetry making the problem two-dimensional in space. Figure 4 shows the two dimensional soil matrix.

When equation (16) is applied to the boundary conditions described in Figure 4 and $\text{Div.}(K.\nabla.Z.) = \frac{\partial K.}{\partial Z.}$, then equation (16) may be written as

$$\text{Div.}(-K.\nabla.P.) + \frac{\partial K.}{\partial Z.} = \frac{\partial S.}{\partial t.} \quad (21)$$

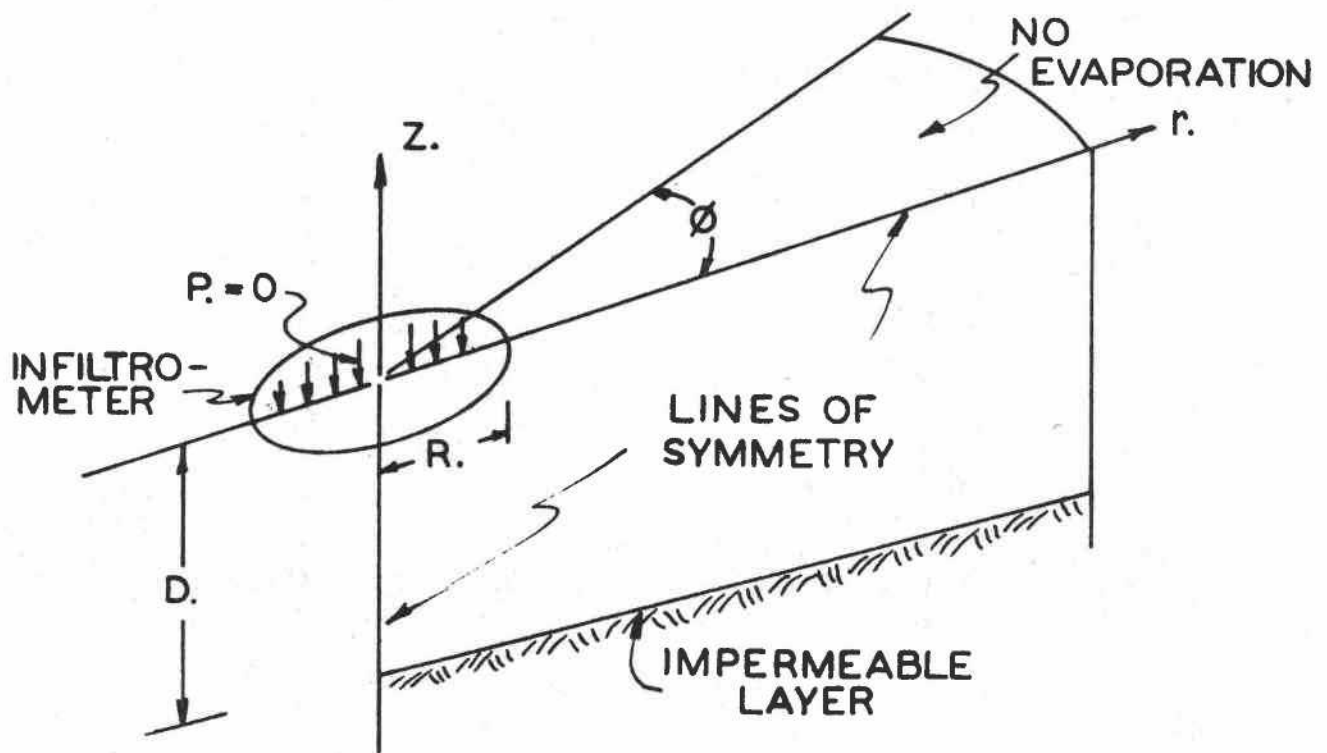


Figure 3. Schematic sketch of the boundary conditions for axisymmetric infiltration into a soil mass from a circular source.

or when the independent variable is written in terms of scaled saturation, equation (21) reduces to

$$\text{Div.} \left(-K. \frac{dP.}{dS.} \nabla. S. \right) + \frac{dK.}{dS.} \frac{\partial S.}{\partial Z.} = \frac{\partial S.}{\partial t.} \quad (22)$$

Since scaled diffusivity, D., is defined by

$$D. (S.) = -K. (S.) \frac{dP. (S.)}{dS.} \quad (23)$$

then equation (22) may be expanded to

$$\frac{dD.}{dS.} (\nabla. S.) \cdot (\nabla. S.) + D. (\nabla.^2 S.) + \frac{dK.}{dS.} \frac{\partial S.}{\partial Z.} = \frac{\partial S.}{\partial t.}$$

or in cylindrical coordinate component form it becomes

$$\begin{aligned} & \frac{dD.}{dS.} \left[\left(\frac{\partial S.}{\partial r.} \right)^2 + \frac{1}{r.^2} \left(\frac{\partial S.}{\partial \phi.} \right)^2 + \left(\frac{\partial S.}{\partial Z.} \right)^2 \right] \\ & + D. \left[\frac{1}{r.} \frac{\partial}{\partial r.} \left(r. \frac{\partial S.}{\partial r.} \right) + \frac{1}{r.^2} \frac{\partial^2 S.}{\partial \phi.^2} + \frac{\partial^2 S.}{\partial Z.^2} \right] \\ & + \frac{dK.}{dS.} \frac{\partial S.}{\partial Z.} = \frac{\partial S.}{\partial t.} \end{aligned} \quad (24)$$

The axisymmetry of the problem reduces equation (24) to

$$\begin{aligned} & \frac{dD.}{dS.} \left[\left(\frac{\partial S.}{\partial r.} \right)^2 + \left(\frac{\partial S.}{\partial Z.} \right)^2 \right] + D. \left[\frac{1}{r.} \frac{\partial}{\partial r.} \left(r. \frac{\partial S.}{\partial r.} \right) + \frac{\partial^2 S.}{\partial Z.^2} \right] \\ & + \frac{dK.}{dS.} \frac{\partial S.}{\partial Z.} = \frac{\partial S.}{\partial t.} \end{aligned} \quad (25)$$

Because of the dependence of D. and K. on S., equation (23) is nonlinear. The use of a mean diffusivity and permeability in equation (23) would reduce

it to a linear diffusion type parabolic equation. Therefore, any solution of (23) in terms of finite differencing may be approached by stability and convergence criteria developed for linear parabolic equations as given by Ames (1965).

If an explicit scheme is used to solve a finite difference approximation to (25), a necessary and sufficient condition for stability of a diffusion parabolic equation in two space variables having equal increments ΔX , is that the time step ΔT must obey the inequality.

$$\Delta T \leq \frac{(\Delta X)^2}{4D.} \quad (26)$$

This illustrates the fact that the time step not only depends on the space increment but on the solution being obtained (Saul'yev, 1964). The inequality will be obeyed if ΔT is given by

$$\Delta T = \frac{(\Delta X)^2}{4D_{\max}} \quad (27)$$

where D_{\max} is the maximum value of the diffusivity $D.(S.)$ on the interval of solution S .

Taking central differences for space derivatives for linear parabolic equations produces second order discretization errors. For nonlinear equations the error may be determined by halving the step size until the functional relation between step size and solution is obtained as shown by Saul'yev (1964). This type of error analysis was taken for the equation in question and it was determined that the total error was of first order. Therefore, the space increment was taken small to give balance between discretization error and roundoff error. The discretization error decreases

with decreasing step size while the roundoff error increases with decreasing step size (Ames, 1965).

Convergence of an explicit scheme is interrelated with stability. Convergence of an implicate scheme requires an error analysis on the time step also (Saul'yev, 1964).

Solutions of equation (25) depend on the functional relationship D.(S.) and K.(S.). Several different types were tried producing different results. The functional relationships

$$\begin{cases} D.(S.) = \frac{1}{\lambda} S.^{1/\lambda + 2} \\ K.(S.) = S.^{2/\lambda + 3} \end{cases} \quad (28)$$

and

$$\begin{cases} D.(S.) = \frac{a^{1/\lambda}}{\lambda} \left(\frac{b}{a}\right)^{2/\lambda + 3} S.^{1/\lambda + 2} \\ K.(S.) = \left(\frac{b}{a}\right)^{2/\lambda + 3} S.^{2/\lambda + 3} \end{cases} \quad (29)$$

yield the best results. The nature of these functions and determination of the constants is discussed in another section of this report.

If $S_n(i,j)$ is the scaled saturation for the next time step at the i,j^{th} grid point of the soil matrix ($i = 1 + (\text{depth} - Z.)\Delta X$ and $j = 1 + r./\Delta X$) and $s(i,j)$ is the scaled saturation for the current time step, the equation

$$\begin{aligned} S_n(i,j) = S(i,j) + \frac{\Delta T}{(\Delta X)^2} & \left[\frac{1}{4} \frac{dD.\{S.(i,j)\}}{dS.} \left[\{S(i,j+1) - S(i,j-1)\}^2 \right. \right. \\ & \left. \left. + \{S(i+1,j) - S(i-1,j)\}^2 \right] + D.\{S(i,j)\} \left[\left(1 - \frac{\Delta X}{2r_j}\right) S(i,j-1) \right. \right. \end{aligned}$$

$$\begin{aligned}
& + \left(1 + \frac{\Delta X}{2r_j} \right) S(i, j+1) + S(i-1, j) + S(i+1, j) - 4S(i, j) \Big] \\
& + \frac{\Delta X}{2} \frac{dK}{dS} \cdot \{S(i, j)\} \left[S(i-1, j) - S(i+1, j) \right] \Big) \quad (30)
\end{aligned}$$

may be used to determine the saturation matrix at the next time step.

The finite difference equation for the upper boundary beyond the radius of infiltration and for the lower impervious boundary is obtained from (30) by setting

$$S(i-1, j) = S(i+1, j) \quad (31)$$

Within the radius of infiltration the upper boundary condition is $S(i, j) = \text{constant}$, which is given as $S. = 1$ or $S. = a/b$ when $P = 0$.

At the axis of symmetry where $r. = 0$, $S_n(i, 1) = S_n(i, 2)$. The outer boundary is at $r. = \infty$.

The above difference equations provide a finite difference approximation to the solution of the boundary value problem given by equation (25) and the boundaries described in Figure 4. The shape and advance of the wetting front may be seen by observing the distribution of moisture in the saturation matrix.

The scaled flux $q.$ may also be obtained from the saturation matrix by noting that it may be defined by

$$q. = \frac{1}{\pi(R.)^2} \iiint_{\Omega.} \frac{dS.}{dt} d\Omega. \quad (32)$$

where $R.$ is the scaled radius of infiltration and $\Omega.$ is the scaled volume of the soil matrix.

The quality q . may be determined numerically from the equation

$$\begin{aligned}
 q. &= \frac{2\pi}{\pi(R.)^2} \sum_{j=1}^m \sum_{i=1}^n \frac{\{S_n(i,j)r_j(\Delta X)^2 - S(i,j)r_j(\Delta X)^2\}}{DT} \\
 &= \frac{2(\Delta X)^2}{(R.)^2 \Delta T} \left[\sum_{j=1}^m \sum_{i=1}^n S_n(i,j)r_j - \sum_{j=1}^m \sum_{i=1}^n S(i,j)r_j \right].
 \end{aligned}
 \tag{33}$$

PROCEDURES

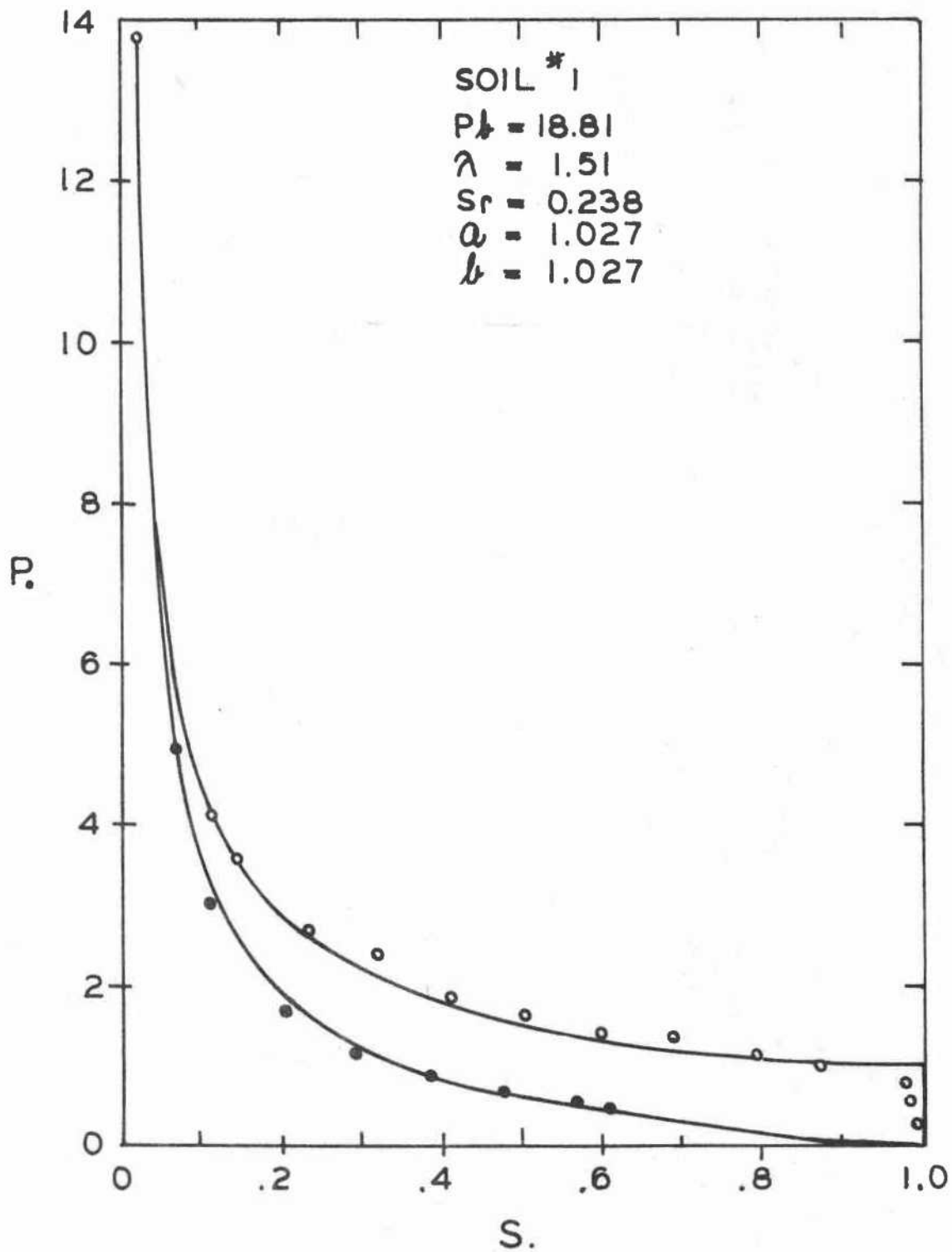
Experimental

Some axisymmetric experimental data were obtained on fragmented soils that were placed in a large diameter laboratory column. The data was obtained for the purpose of observing, in qualitative terms, the wetting patterns and infiltration capacity curves for the two media shown in Figures 5 and 6 that have a wide range of characteristics. Since the imbibition function of the model has not been perfected, a comparison between the mathematical model and the experimental results from the laboratory column will not be given.

A column 28 cm square and 60 cm deep was constructed of clear acrylic plastic. Fragmented soil was packed into the column to within 5 cm of the top. A 1/4 circle infiltrometer was constructed so that it could be clamped into the corner of the soil column. This configuration represented the soil-infiltrometer section shown schematically in Figure 4 where the angle $\phi = \pi/2$ radians.

A sketch of the infiltrometer is shown in Figure 7. Holes 0.222 cm in diameter were drilled on a triangular spacing of 1.38 cm. The holes were counter-sunk on the inside of the infiltrometer to a depth of 0.3 cm.

Figure 5. Scaled capillary pressure as a function of scaled saturation for soil No. 1 used in the experimental infiltration model. The open circles are drainage data, the closed circles are for imbibition, and the curves represent the theoretical equations.



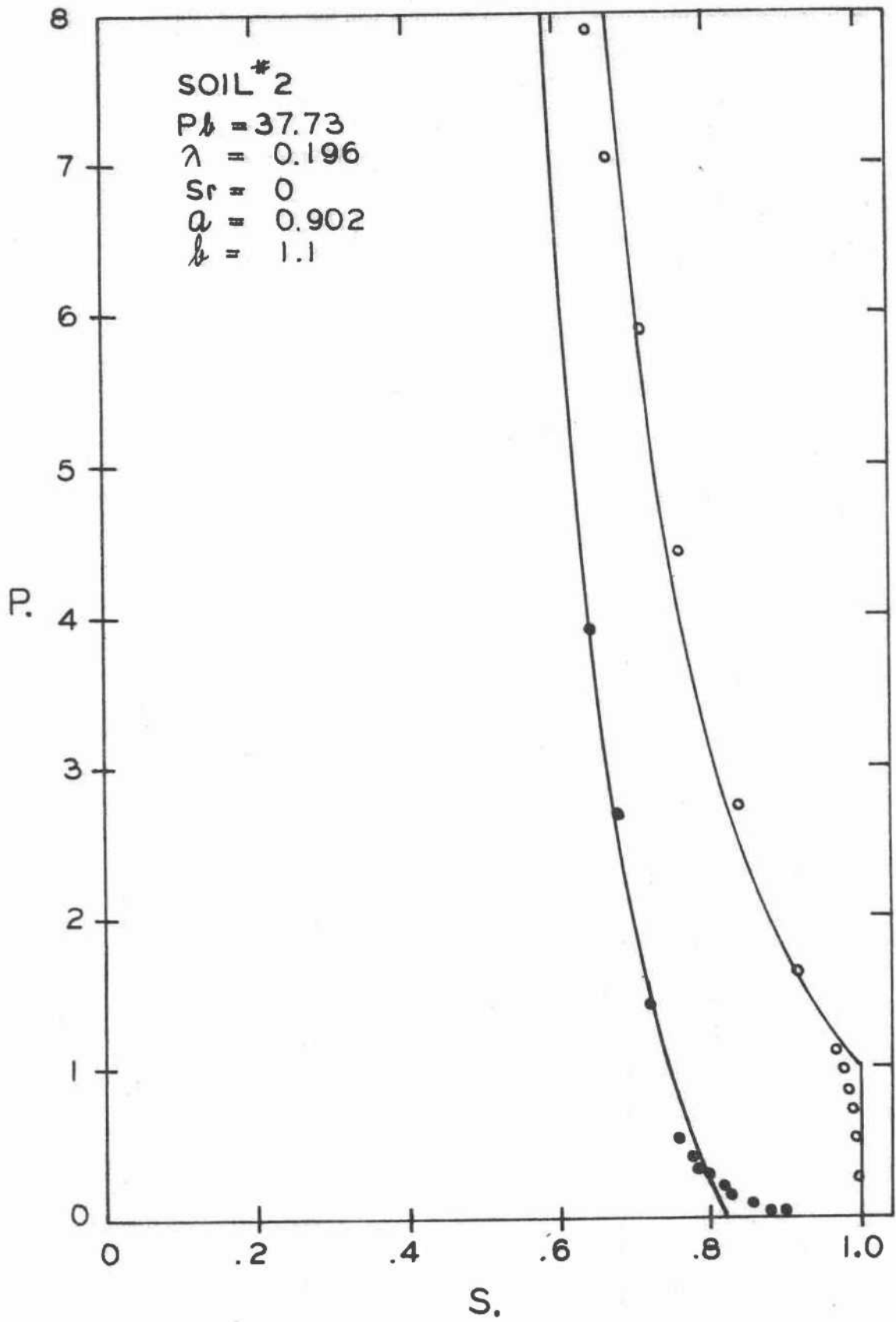


Figure 6. Scaled capillary pressure as a function of scaled saturation for soil No. 2 used in the experimental infiltration model. The open circles are drainage data, the closed circles are for imbibition, and the curves represent the theoretical equations.

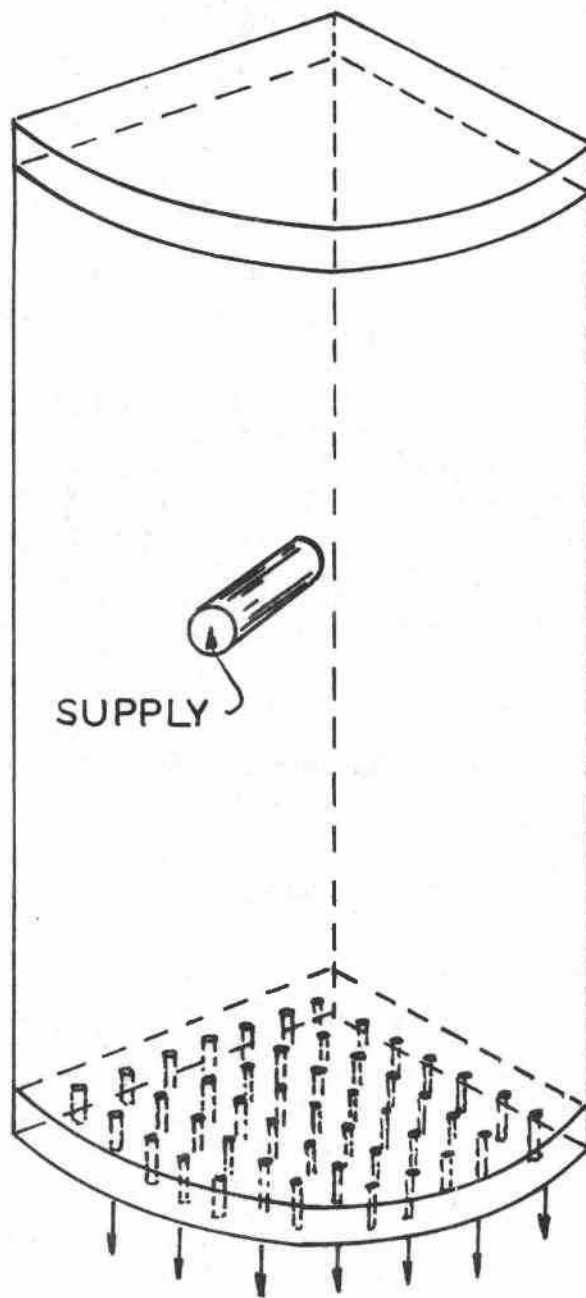


Figure 7. Schematic of experimental infiltrometer.

The entire infiltrometer chamber was filled with water and connected to a supply reservoir through a valve and flow meter. The pressure of the water at the soil surface during infiltration was adjusted by the control valve and maintained at zero by observing the contact zone between the infiltrometer and the soil. When the pressure exceeded zero, water was detected moving from under the infiltrometer to an area larger than the infiltration diameter. When the pressure became less than the bubbling pressure of the holes in the bottom of the infiltrometer, air was sucked into the chamber. Both of these indicators were used to keep the pressure at zero. The flow rate was recorded periodically during the experiment and the wetting fronts were traced on the sides on the column at specified time intervals.

Mathematical Model

The mathematical model was programmed for operation on a digital computer, CD 3300. The program reads in an initial soil moisture distribution matrix which in this study was constant. Once the initial saturation matrix is read in, the program calls for the minimum value of saturation, So, the empirical constants, a, b, and λ , which are called AM by the program, and the scaled radius of infiltration, R.

The program produces the values of t. and q. and the saturation matrix for twenty time steps. At the end of the program the final saturation matrix is stored in a file which may be used at a later time if the continuation of the solution is desired.

RESULTS AND DISCUSSION

The results of this project will be presented under two separate headings, one dealing with the mathematical model and the other with an

experimental model. Even though a great emphasis will be placed on the results of the mathematical model, a large number of physical experiments were made that will not be presented. Two experiments have been selected and will be presented to illustrate some of the problems associated with verification of the theory. As indicated in the preface of this report, the theory presented is only tentative and will be subject to change as more experimental data are collected and the mathematical model is further refined.

MATHEMATICAL MODEL

The various solutions of the mathematical model that are subsequently presented are based upon an a/b value of unity where a and b in equation (19) are 0.85. These results will show largely the effect of the pore size distribution index λ , the initial saturation, S_0 , and the radius of the infiltrometer upon the infiltration rate. These results are shown in Figures 8-12.

The curves shown in Figures 8-9 show the effect of initial and boundary conditions upon the infiltration capacity curve. In Figure 8, the asymptotic infiltration capacity decreases as the diameter of the infiltrometer increases. The curves seem to approach a single infiltration capacity curve for large size infiltrometers or one-dimensional infiltration. In other words, the larger the infiltrometer, the closer the infiltration capacity curve approaches the one-dimensional rate. The size of the infiltrometer needed to measure the true infiltration capacity curves depends upon the magnitude of the bubbling pressure head of the media. If one were to construct an infiltrometer for purposes of measuring one-dimensional infiltration on a wide range of soil profiles, the radius would have to

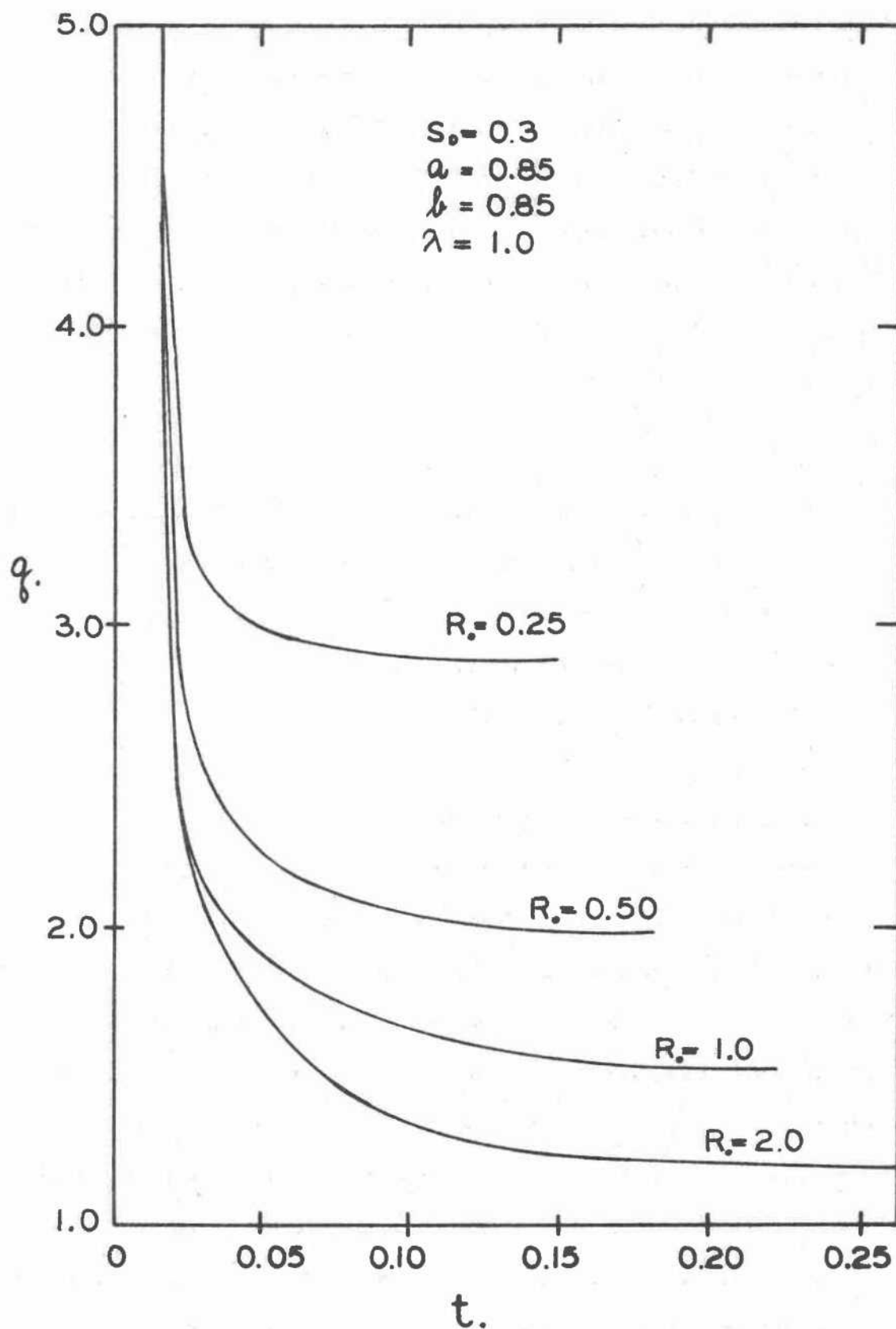
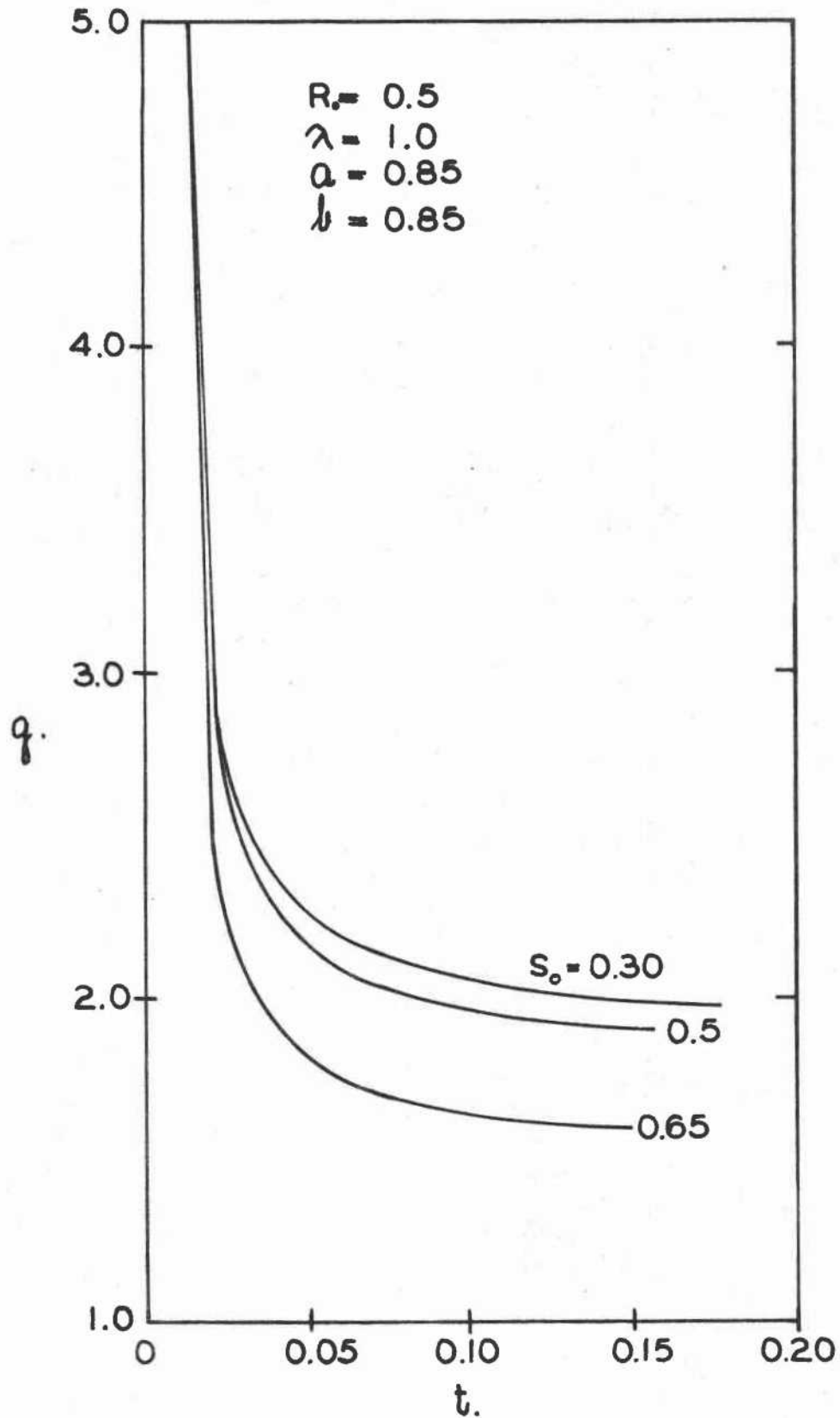


Figure 8. Scaled infiltration rate as a function of scaled time for various sizes of infiltrometers of scaled radius, R_s , obtained from the mathematical model for specified soil properties.

Figure 9. Scaled infiltration rate as a function of scaled time for three different initial saturations, S_0 , obtained from the mathematical model for an infiltrometer of scaled radius equal to 0.5



be at least two or three times the largest bubbling pressure head that one expects to encounter.

In Figure 9, the infiltration capacity is related to the initial water content of the soil. The greater the initial water content, the lower the infiltration rate. At low values of initial water content, the infiltration capacity curves seem to be only slightly affected by the initial water content, that is, the infiltration capacity curve for zero initial water content is probably not greatly different than that for curve $S_0 = 0.3$. The solution of the partial differential equation for initial water contents below 0.3 oscillate with time. They are not reliable and, therefore, are not shown in Figure 9.

The infiltration capacity curves shown in Figure 10 show the influence of the pore size distribution index upon infiltration. The wider the distribution of pore sizes (small values of λ), the higher the infiltration rate and the greater the time required to reach the infiltration capacity. For a given initial condition the infiltration capacity curves for various values of λ are more widely separated when the radius of infiltration is small than when it is large. (Compare Figure 8 with Figure 9 for $\lambda = 1.0$.)

Apparently the lateral spreading of the wetting front is closely related to the pore size distribution index. If the infiltrometer is large, the effect of lateral spreading is insignificant when compared to the vertical movement, and the effect of λ upon the infiltration capacity is not marked.

The distribution of water in the soil profile as a function of time is shown for a particular set of boundary and initial conditions in Figures 11 and 12. In Figure 11, the distribution of water with respect to profile

Figure 10. Scaled infiltration rate as a function of scaled time for various soils having different pore size distributions obtained from the mathematical model for specified initial and boundary conditions.

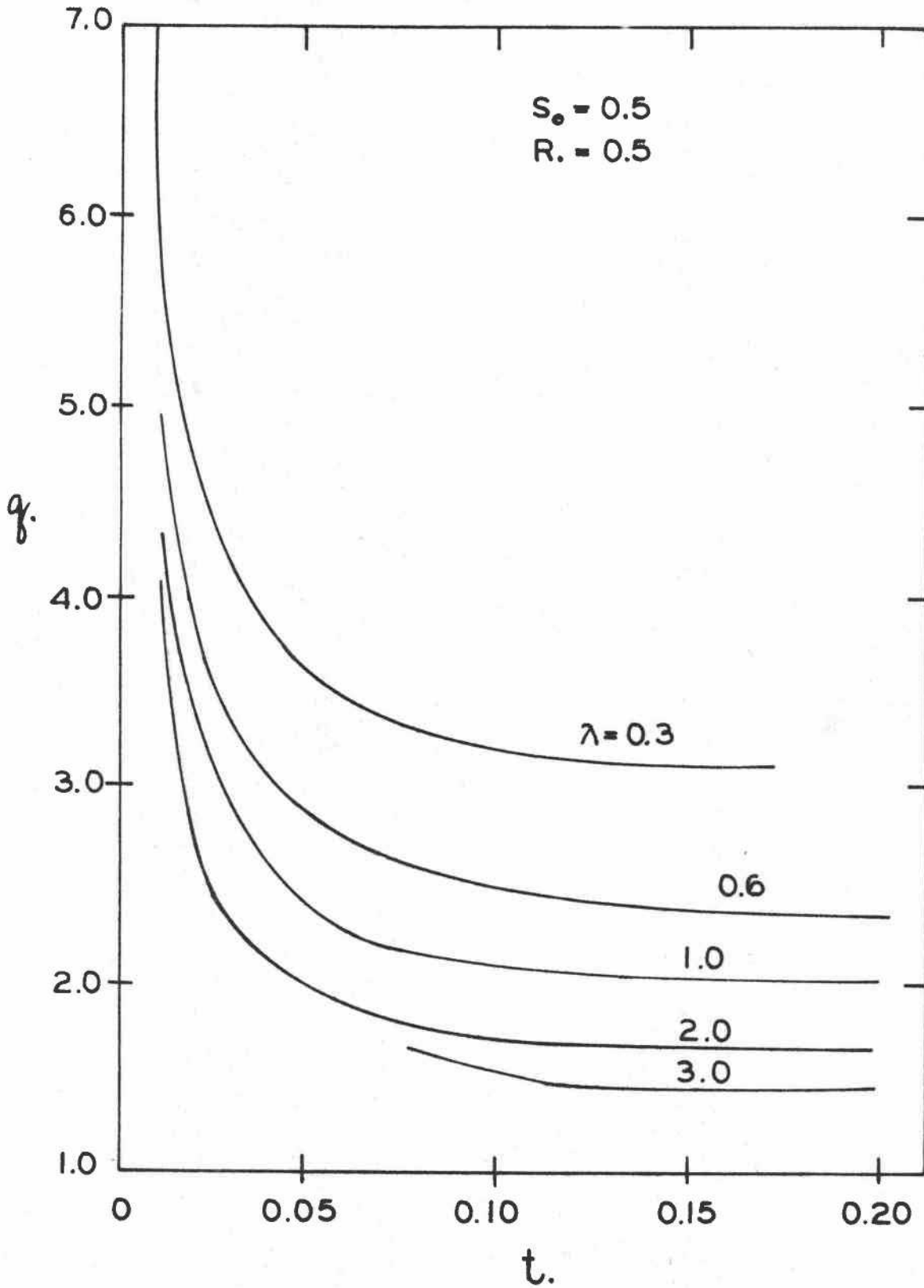
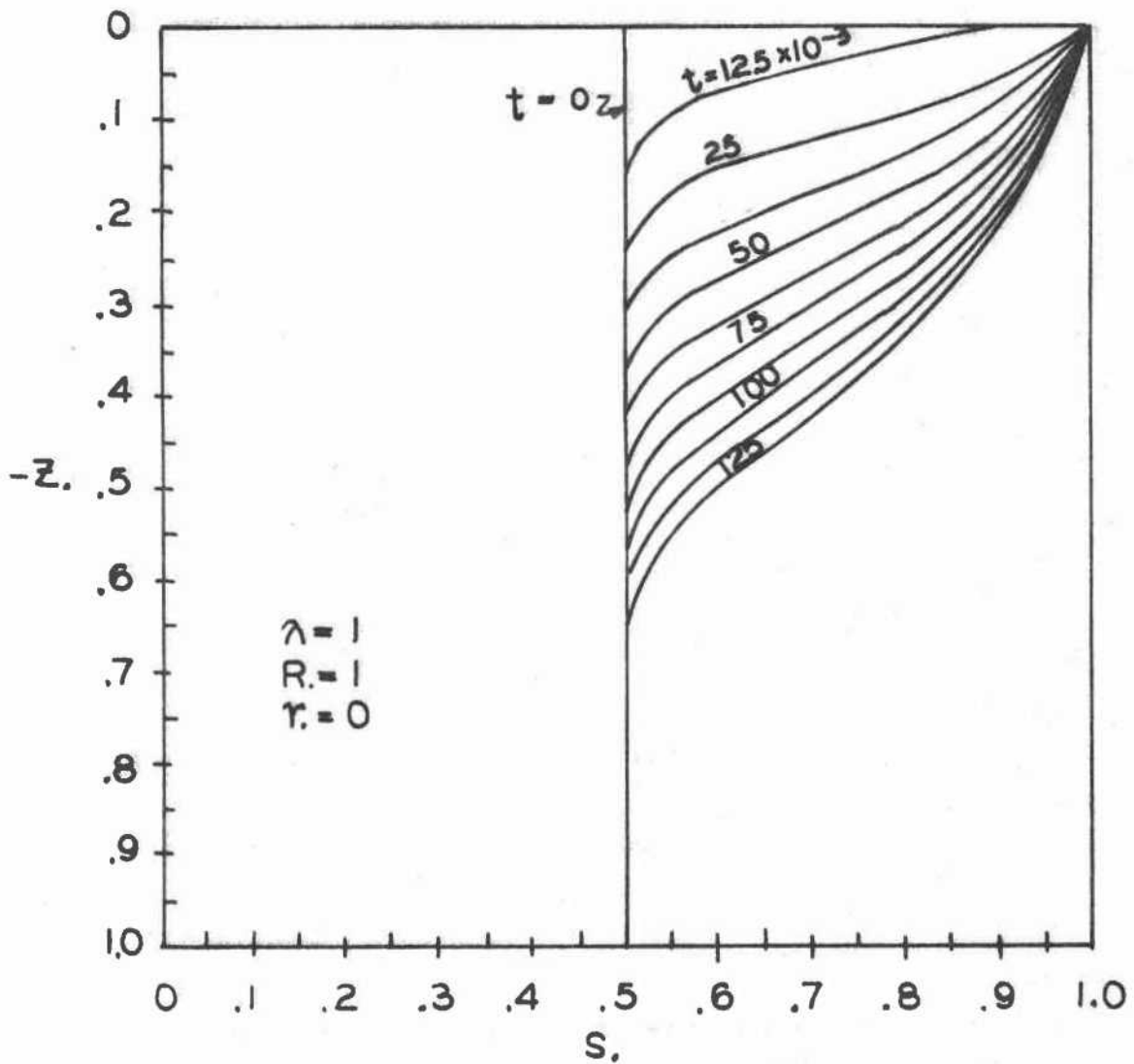


Figure 11. Scaled saturations as a function of scaled depth below the soil surface at the center of the infiltrometer for various times obtained from the mathematical model for the initial and boundary conditions specified in the figure.



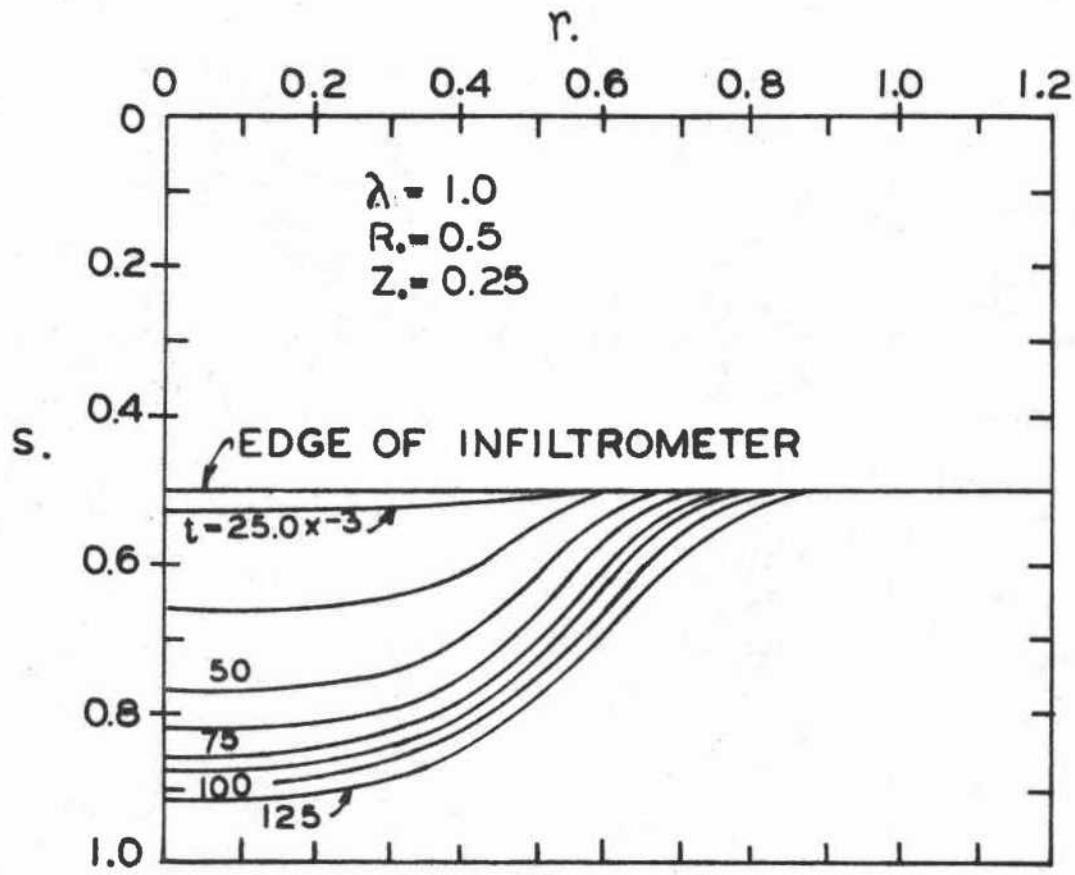
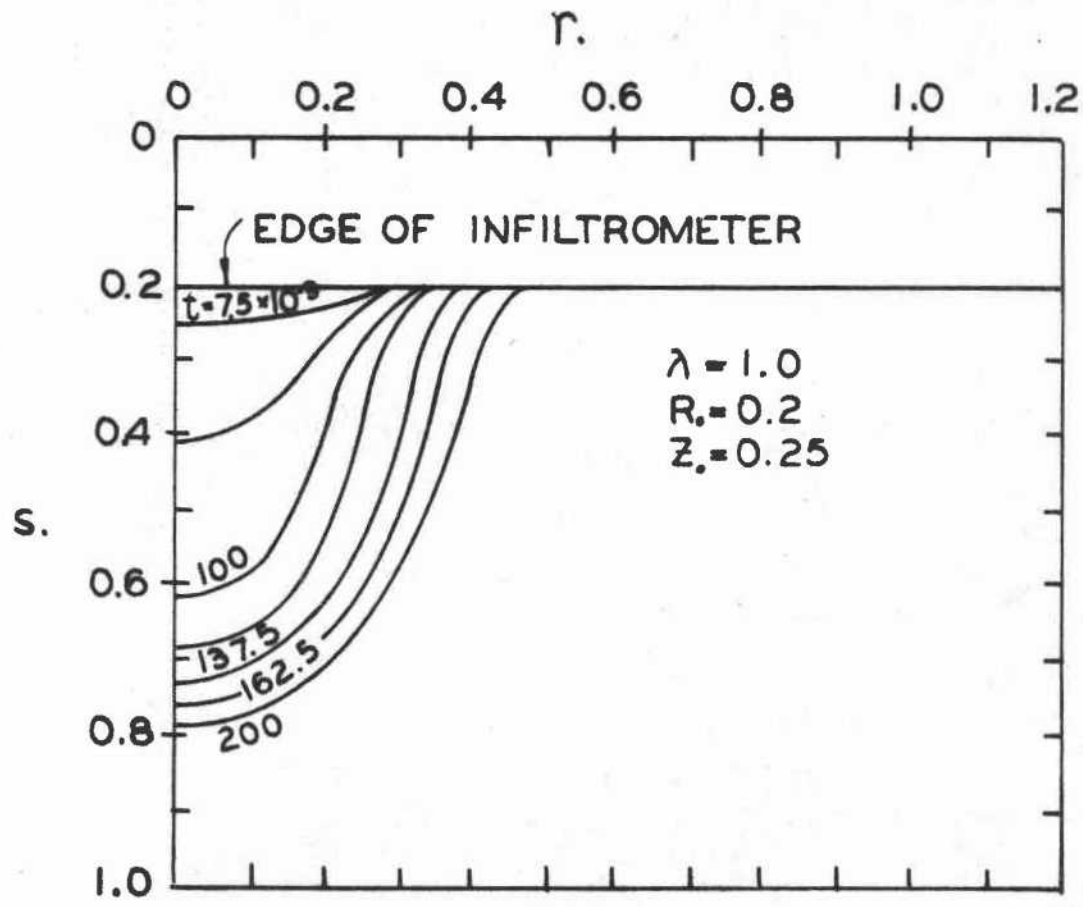


Figure 12. Curves from the mathematical model showing scaled saturation as a function of scaled radial distance from the center of infiltration for various times and for two infiltrmeters.

depth and time under the center of the infiltrometer is shown. The distribution of water with respect to profile depth and time under the center of the infiltrometer is also shown in Figure 11. The distribution of water in the soil as a function of radial distance from the center of the infiltrometer and time is shown in Figure 12 for a small depth below the soil surface.

Large values of R tend to flatter the time curves with respect to depth. Small values of R tend to produce a three-dimensional effect, i.e., to make the wetting front a hemispheroidal shape. Large values of R tend to produce a hemielipsoidal shape.

A comparison of the drainage function in the infiltration model with the imbibition function is shown in Figure 13. Scaled infiltration rate is plotted as a function of scaled time for $\lambda = 1.0$. Since the ratio a/b is unity, the permeability at zero capillary pressure is the same as for a completely saturated media, i.e., no air entrapment occurs. In other words, when the capillary pressure is zero, the permeability of the media is the same for both functions. Only the effect of including the two parameters a and b is shown in Figure 13. The effect of the drainage function is to produce an infiltration capacity that is larger than given by the imbibition function. However, the general conclusions that one would deduce from an analysis of an axisymmetric infiltration model and the drainage function would not be different from that arrived at by using the imbibition function.

When the infiltration capacity is plotted as a function of radius of infiltration and pore size distribution index, λ , at a low initial saturation, as shown in Figures 14 and 15, the relationship among these variables may

Figure 13. A comparison of the infiltration capacity curve using the drainage function with the curve obtained using the imbibition function in the mathematical model.

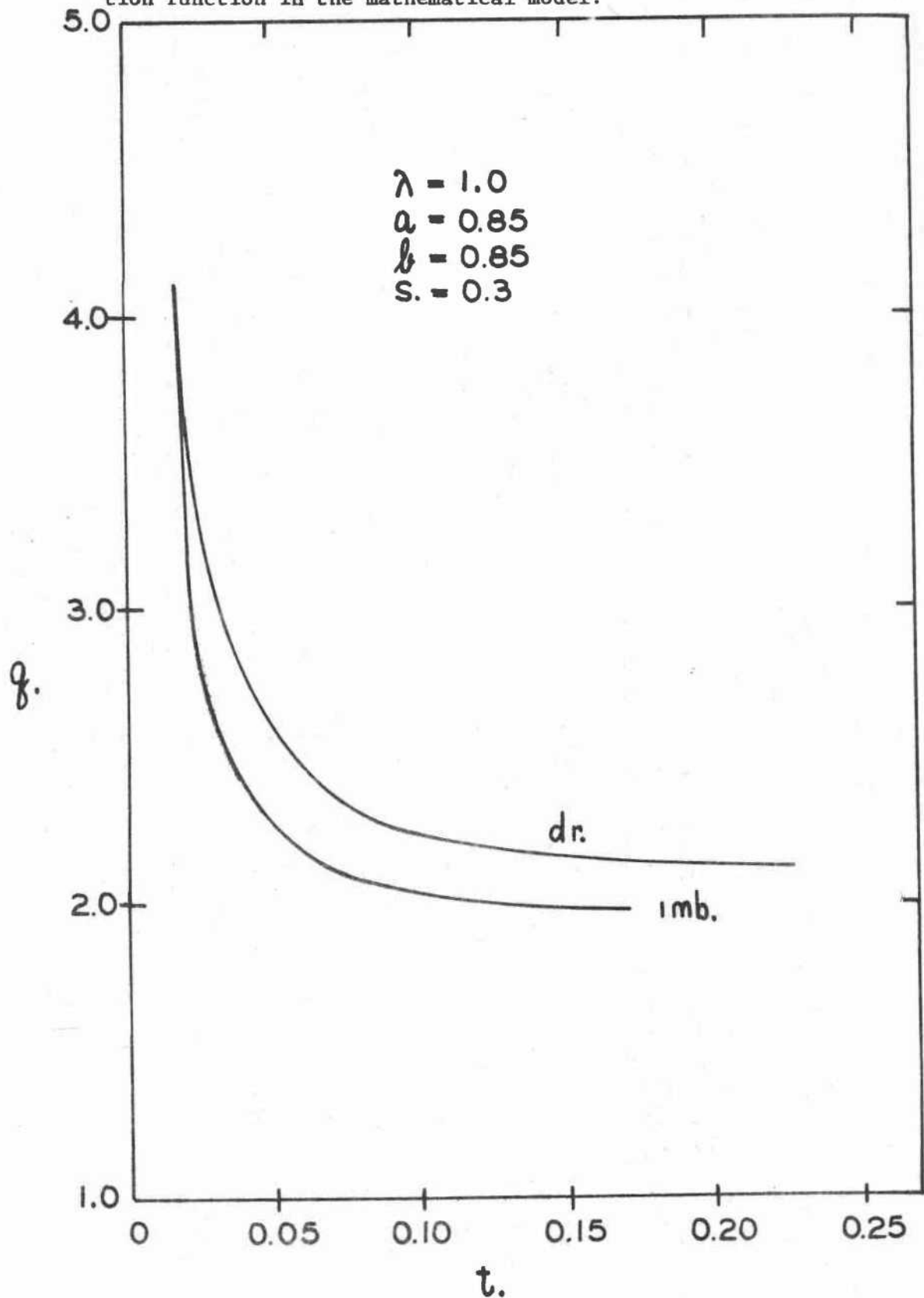
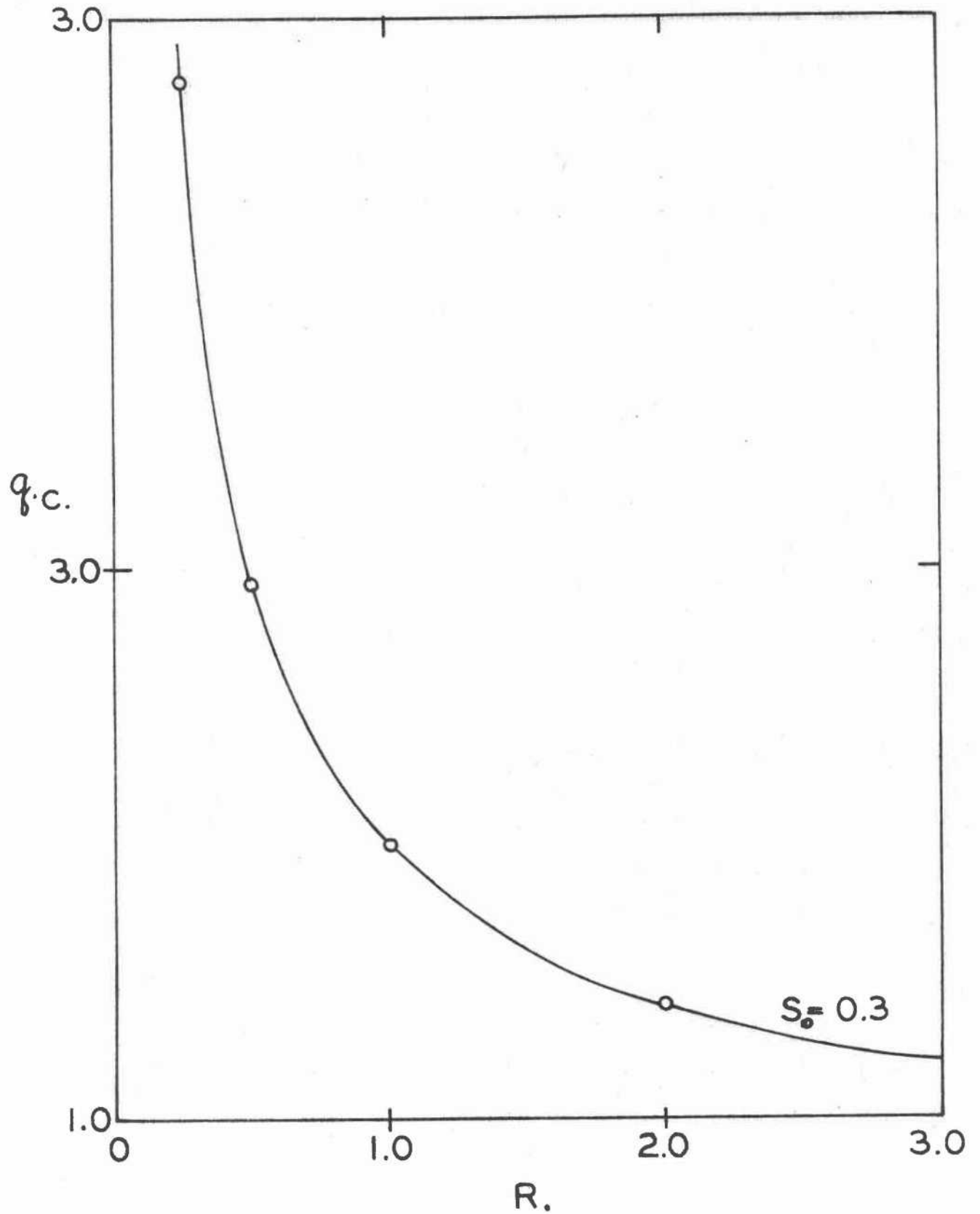


Figure 14. Theoretical scaled infiltration capacity as a function of scaled size of infiltrometer for $\lambda = 1$ and $S_0 = 0.3$.



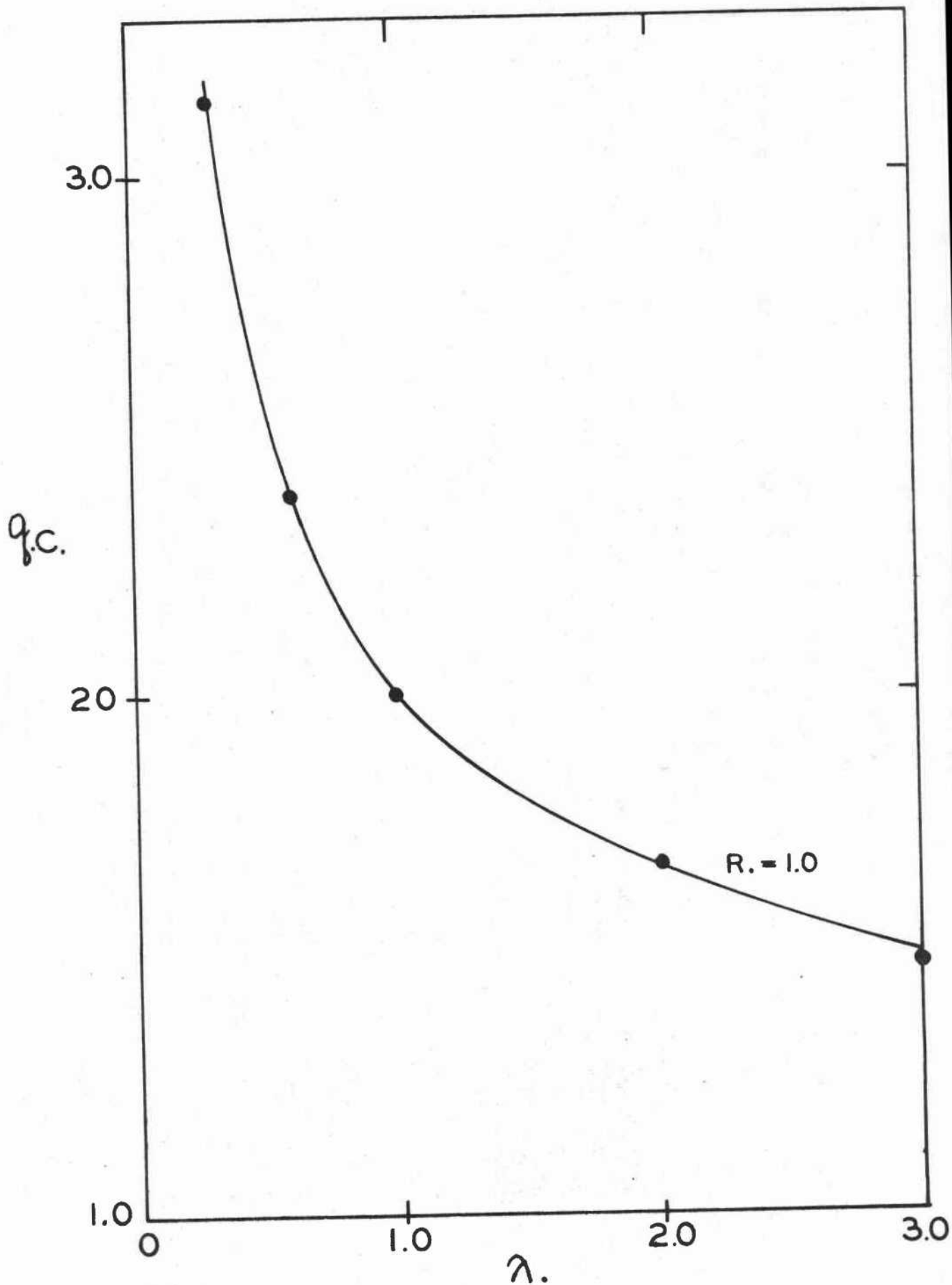


Figure 15. Theoretical scaled infiltration capacity as a function of pore size distribution index for a scaled infiltrrometer radius of 1.0 and initial scaled saturation of 0.3.

be established. To a first approximation, infiltration capacity may be obtained from the equation

$$q_c = 1 + \frac{1}{2R\lambda^{3/4}} \quad (34)$$

At this stage of theoretical development of the theory, equation (34) is only approximate for reasons previously mentioned and because the initial saturation has been excluded in the expression. Since the mathematical model is not capable of producing solutions at low initial saturations, the approximate form of how the initial saturation affects the infiltration capacity is shown in Figure 16. The verification of the model and theory presented here is the subject of future research funded under a grant from the Department of Interior, Office of Water Resources Research.

Some experimental work was performed under this project and the results are presented in the following section.

EXPERIMENTAL MODEL

Results from the axisymmetric column experiment are shown in Figures 17-21. Two media having widely different characteristics were selected to qualitatively evaluate the results from the mathematical model. The capillary pressure-saturation curves for these two media are shown in Figures 5 and 6. The data are shown as points, while the curves were obtained from equations (19) and (8) for the imbibition and drainage functions respectively. The ratio of bubbling pressures for these media are approximately 2:1. The size of the infiltrometer for soil No. 1 was 1.8 cm and for soil No. 2 it was 5.5 cm or in the ratio of 3:1. Therefore, the laws of similitude were not exactly satisfied and comparisons between the two

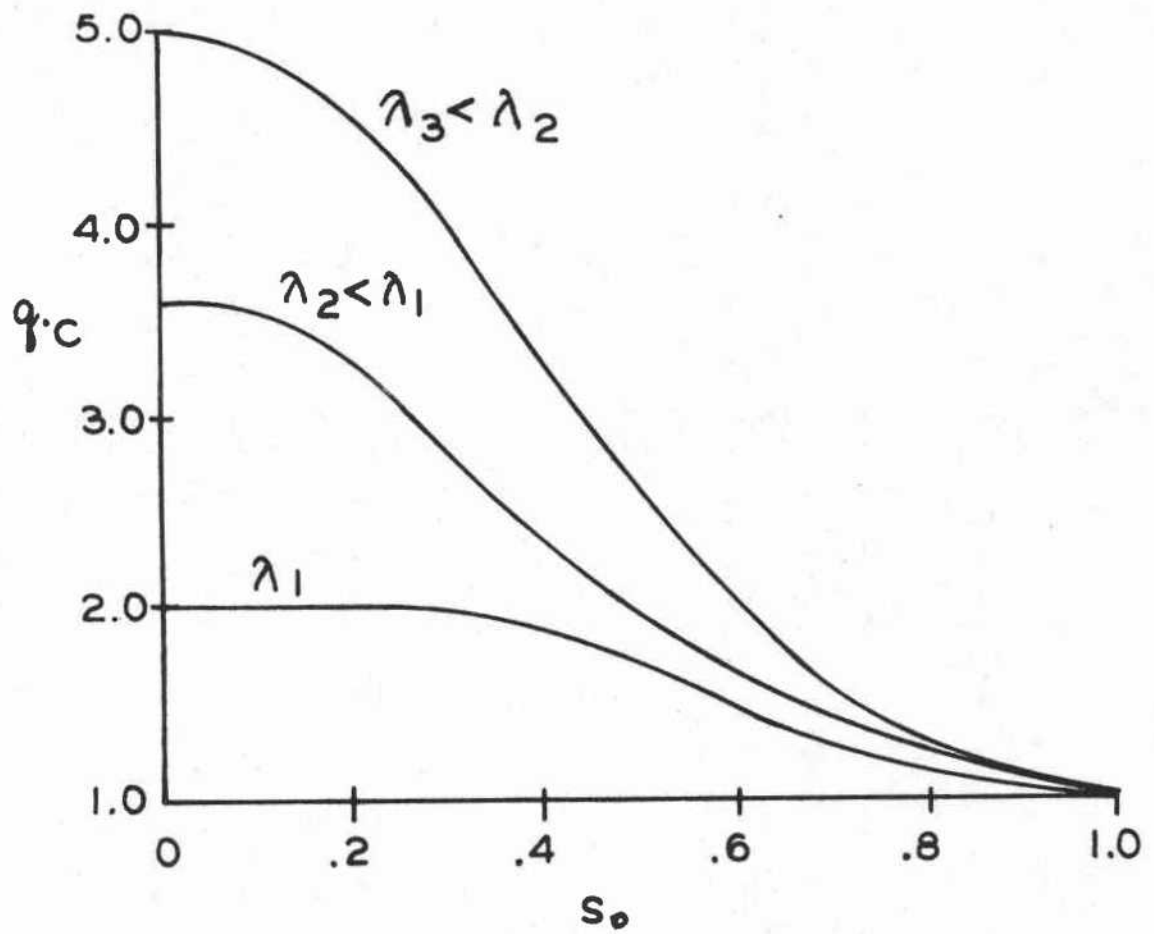


Figure 16. Proposed relationship of infiltration capacity as a function of scaled initial saturation, S_o , for a range of soils where the radius of infiltration is fixed.

media are not easily made. Nevertheless, the data are presented and additional studies are planned for future research.

The wetting front patterns for these two soils are shown in Figure 17 in terms of scaled depth and radius for various times. Only the largest time pattern for soil No. 2 (shown as a dashed curve) is given. All other time curves for soil No. 2 are smaller than the one shown. The solid curves are for soil No. 1.

These wetting front patterns can be compared only for the same scaled time. However, the physical size of the model did not permit the infiltration experiment for soil No. 2 to be continued for large values of scaled time without the wetting front coming in contact with the boundaries of the model. The ratio of scaled times for these two media are 1600:1. The absolute values of the wetting pattern distribution for soil No. 2 are shown in Figures 18 for real time in seconds.

The advance of the wetting fronts under the center of the infiltrometer for these two soils are shown in Figure 19. For soil No. 2, the values of Z . and t . were multiplied by 10 before plotting so that the two soils could be presented on the same plot. Obviously, this procedure in no way affects the slope of the Z . - \sqrt{t} . curve. The rate of advance of the wetting front for soil No. 2 is considerably greater than for soil No. 1, which has a large value of λ . The relative depth of wetting for the same scaled time is greater for soils having structure than for sands that are structureless.

Scaled infiltration rate as a function of scaled time is shown in Figure 20 for soil No's 1 and 2. The range of measured times for soil No. 2 is so small compared to soil No. 1 that the last three largest time

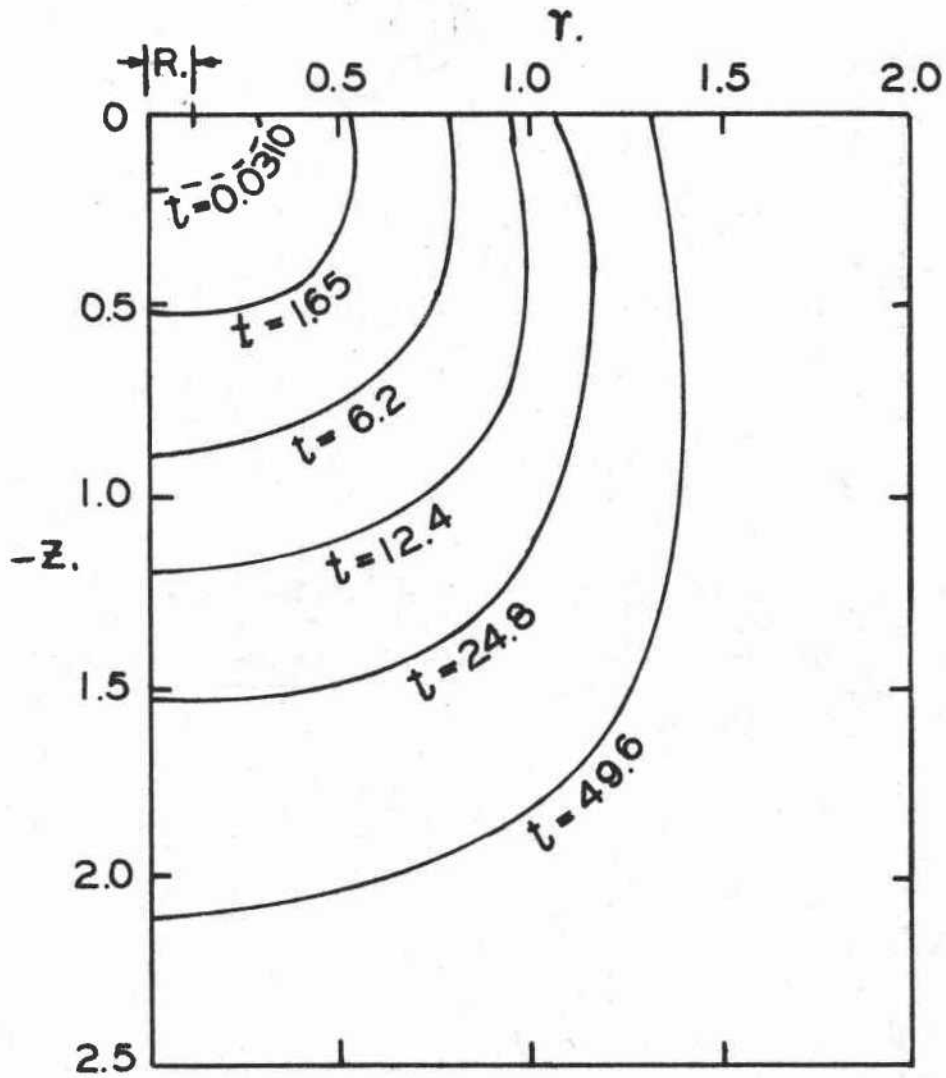


Figure 17. Experimentally determined wetting front distribution patterns for soil No.'s 1 and 2, plotted in terms of scaled depth below the soil surface and scaled horizontal distance from center of infiltration. The dashed curve is for soil No. 2.

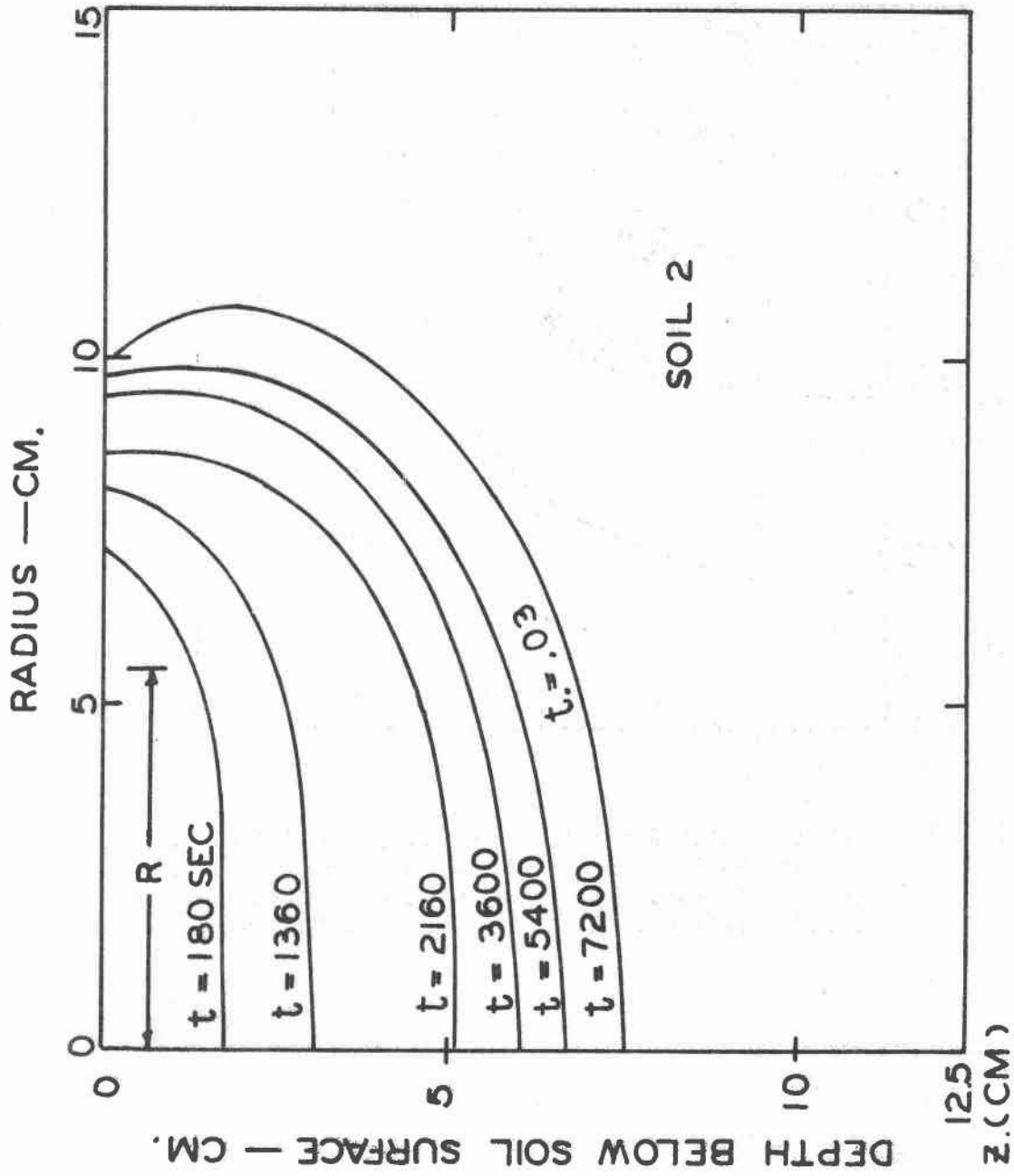


Figure 18. Experimentally determined wetting front distribution patterns for soil No. 2 plotted as a function of depth below the soil surface and horizontal distance from the center of infiltration for various times.

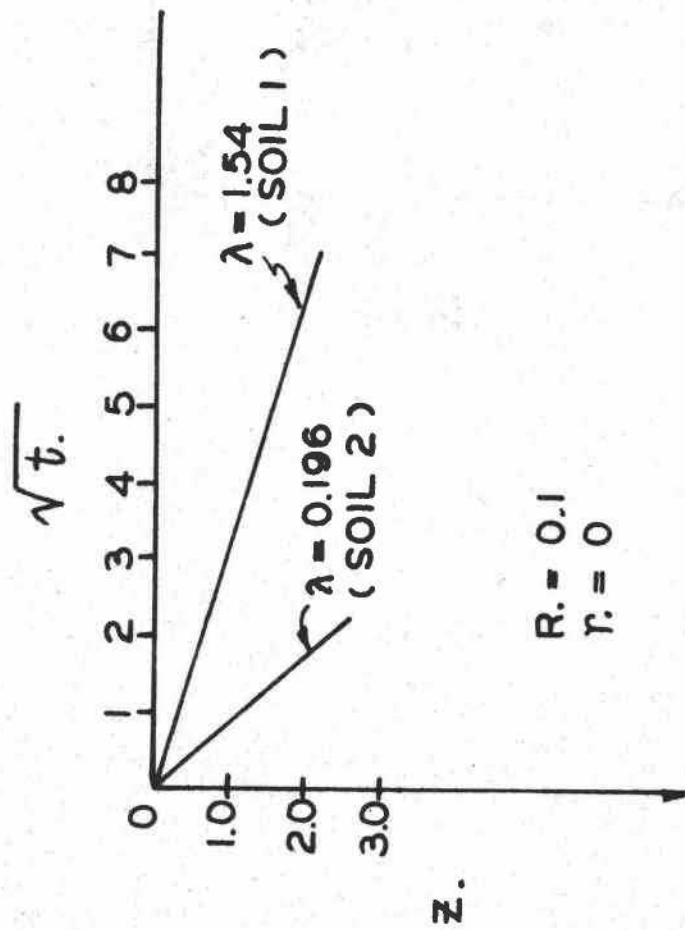
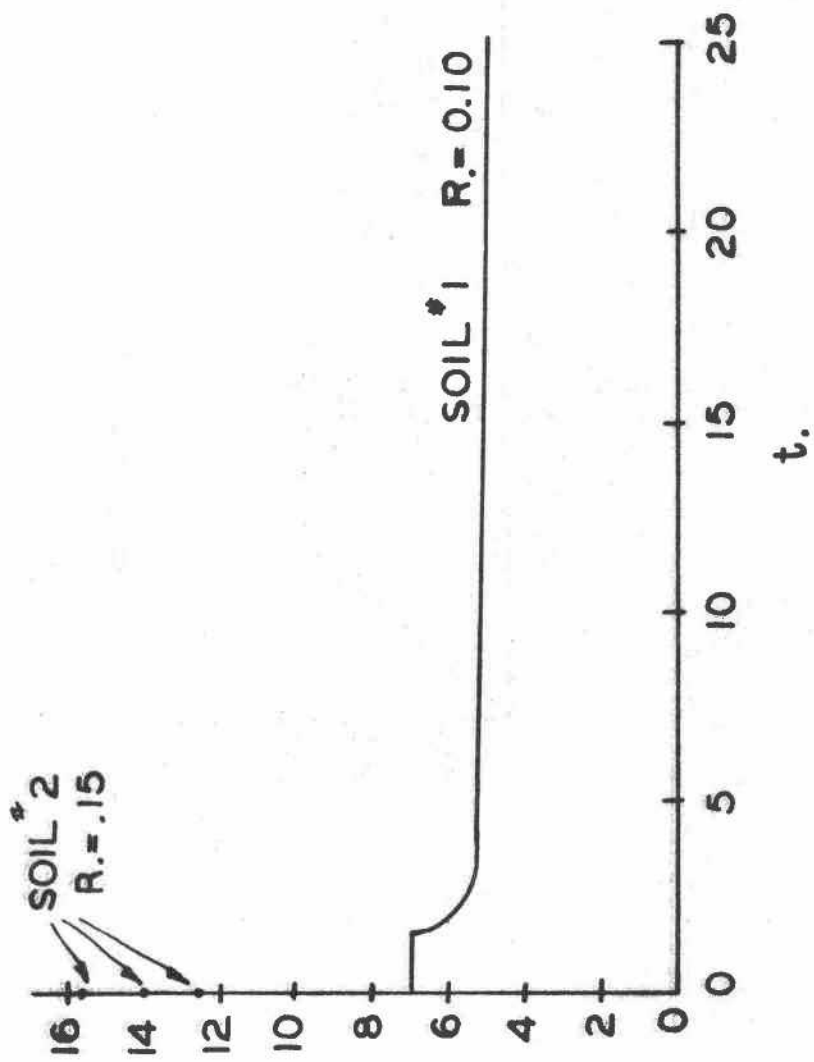


Figure 19. Wetting front advance for soil No.'s 1 and 2 under the center of the infiltrometer. The data points for soil No. 2 were multiplied by 10 before plotting.

Figure 20. Scaled infiltration rate as a function of scaled time for the two soils used in the experimental infiltration model.



values are shown along the zero time line in Figure 20. Obviously, soil No. 2 had not reached its infiltration capacity and cannot be compared with soil No. 1. Unless experimental results are compared in terms of scaled variables the results may be completely misleading. For example, when scaled infiltration rate is plotted as a function of scaled time on a much smaller scale (without considering the time scale for soil No. 1), the infiltration capacity seems to be reached in a relatively short period of time as seen from Figure 21. However, when this infiltration rate is compared with soil No. 1, much larger values of time are required to reach the infiltration capacity. Other things being equal, the infiltration capacity for soil No. 2 should be much larger than soil No. 1 since the λ values are 0.2 and 1.5 respectively.

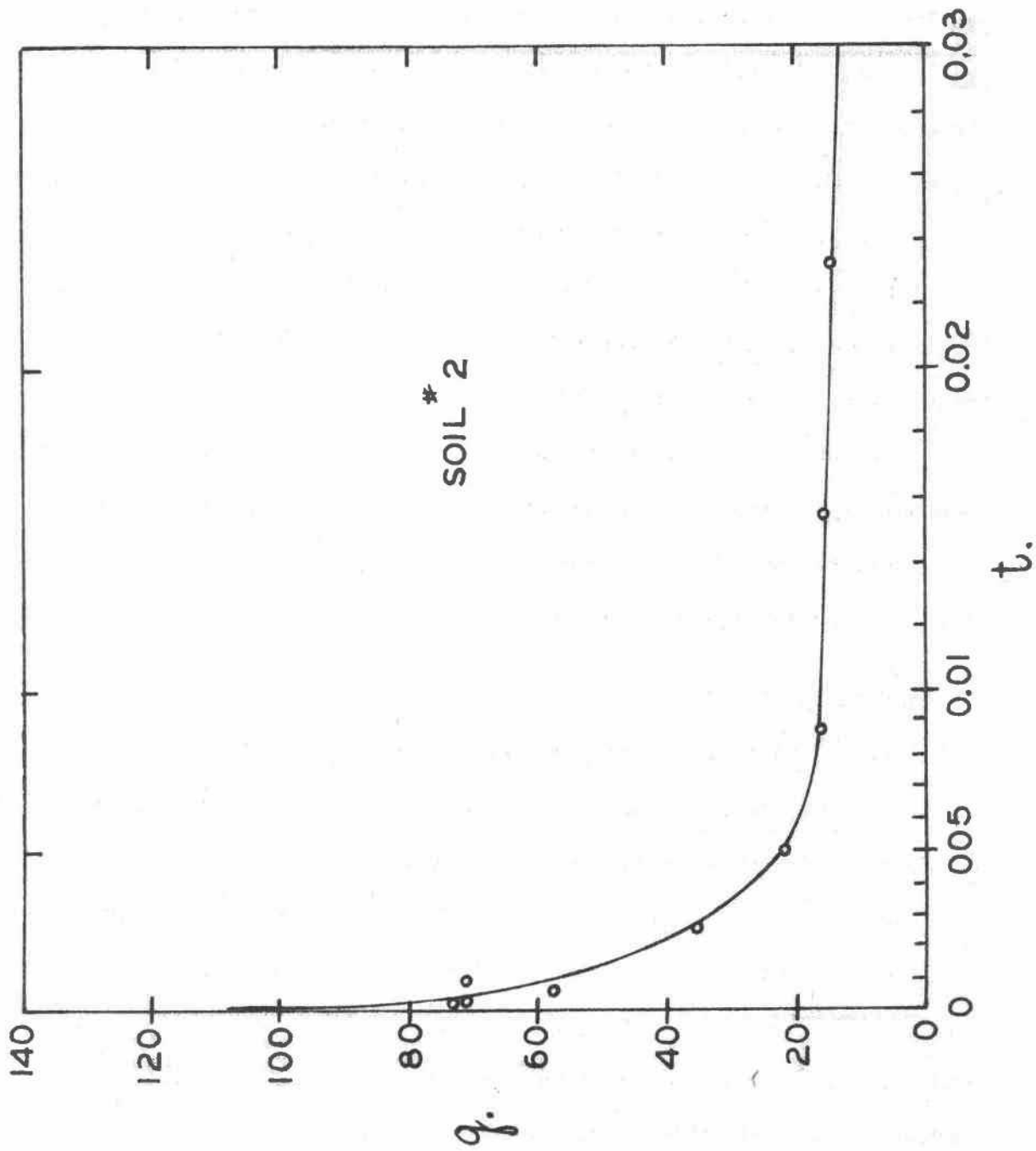
The permeability value needed to compute scaled time was measured independently in small column experiments. All other hydraulic properties for these two soils were obtained from the capillary pressure-saturation curves shown in Figures 5 and 6.

SUMMARY AND CONCLUSIONS

The hydrologist or land manager is often faced with the problem of selecting equipment and methods that can be used to gather data for purposes of making wise decisions and accurate predictions of the watershed.

Watershed infiltration is one of the most important processes that occur on the watershed, as it has a considerable effect on runoff from precipitation, yield of vegetation, erosion, etc. Usually field infiltration data are obtained for determining infiltration rates that occur due to precipitation and other properties of the soil that effect water movement.

Figure 21. Experimental scaled infiltration rate as a function of scaled time for soil No. 2 plotted on expanded graph scales.



The selection of the best possible techniques and equipment for collecting infiltration data is of great concern.

The field investigator may choose on the one hand a large scale infiltrometer that approaches the conditions that may occur during precipitation. Often these infiltrometers are cumbersome, awkward, and uneconomical to use. However, they may provide excellent data for making accurate runoff predictions. Also, they have the advantage that infiltration is measured on a relatively large surface area. On the other hand, small scale infiltrometers using simple techniques and equipment (such as a simple ring for creating a constant source of water) may be used to obtain infiltration data. The data is easily obtained and the equipment is economical to use. One major disadvantage is that the data are very difficult to interpret.

Axisymmetric infiltration using relatively small infiltrometers and simple boundary conditions was studied through the use of general soil-water relationships. These relationships provide a means for interpreting field infiltration data using small scale infiltrometers. These relationships cover a wide range of soil properties and permit a standard to be constructed for making comparisons and interpretations.

Infiltration of water into the soil from a circular source at the soil surface was studied through the use of the diffusivity equation. The soil surface in contact with the source was maintained at complete saturation or zero capillary pressure. The effects of soil hydraulic properties, initial soil-water content, and size of infiltrometer were studied using the mathematical model.

The results shown and discussed are far from conclusive and the final theory remains to be developed, but the study has produced results that

will be very helpful in the interpretation of infiltration data in qualitative terms. Indeed, this study has opened up a number of areas that are presently being studied in an attempt to obtain a simple field measurement technique that will be useful in making runoff predictions.

These results may be used for determining the hydraulic properties of the soil which in turn can be used to construct an infiltration curve for one-dimensional infiltration during precipitation on the watershed. In other words, once the hydraulic soil properties are determined then techniques for constructing a one-dimensional watershed infiltration curve during precipitation can be used, e.g., Mein and Larson (1973). These one-dimensional models lend themselves to easier handling of more complicated boundary and initial conditions that may be considered on the watershed during the precipitation event.

The interpretation of axisymmetric infiltration cannot be adequately treated without consideration of similitude criteria for flow of water in soils. All of the data are presented in terms of scaled variables. The general relationship among infiltration capacity, pore size distribution, and size of infiltrometer given by equation (34) is based upon selecting the asymptotic infiltration rate. The scales that are chosen to plot the data are very important and if not properly selected, may result in incorrect conclusions.

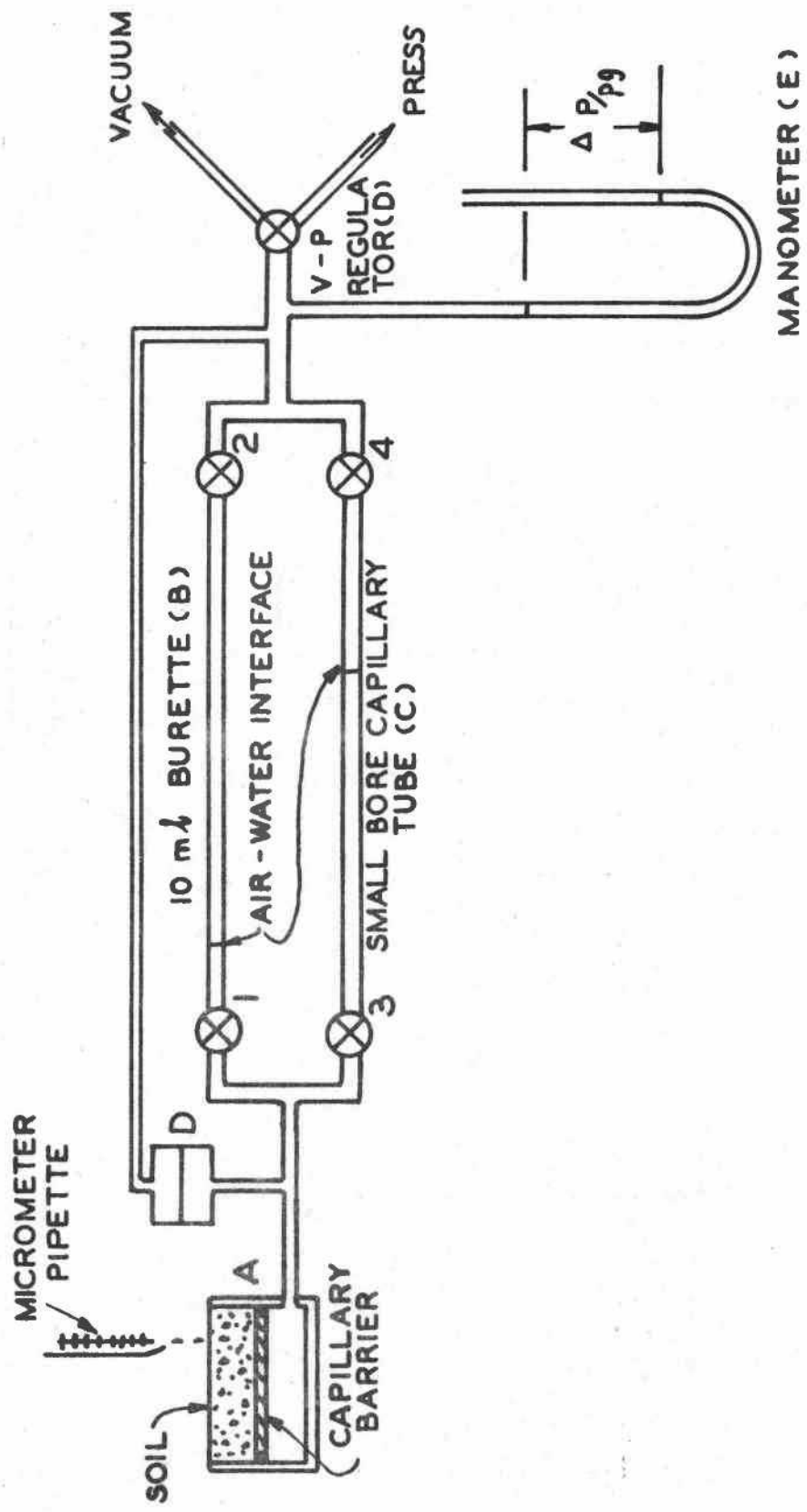
The experimental infiltration data for two widely different soil materials were used to illustrate this difficulty. Scaled infiltration rate was plotted as a function of scaled time from the experiment. The scaled variables were determined from actual measurement of the standard units. What appeared to be an asymptotic infiltration rate on one soil turned out not to be the asymptotic rate when compared with the other.

It may be possible that the time scale for the mathematical model was not sufficiently long to obtain the actual asymptotic infiltration rates. If so, equation (34) may be invalid in a quantitative sense. The general qualitative deductions would probably remain unchanged.

Appendix I

Experimental Method of Determining Capillary Pressure and Saturation for Imbibition and Drainage

The soil sample placed upon the capillary barrier may be either disturbed or undisturbed. After the soil sample has been firmly packed or brought in contact with the capillary barrier, the apparatus (A) is vacuum saturated (being careful to hold the soil firmly in place during saturation). The fully saturated soil sample holder (A) is connected to the horizontal burette-capillary tubes (B) and (C) with the valves 1 and 3 closed. The transducer (D) is likewise connected to the sample holder being careful to exclude all air bubbles. With valves 1, 2, and 4 open and 3 closed, the vacuum-pressure regulator (D) is adjusted to produce a small vacuum on the manometer (F) so that all excess liquid is removed from the sample. If the sample does not contain a sufficient excess, additional liquid is added to the surface of the soil. Excess liquid is withdrawn from the sample into the horizontal burette until the air-liquid interface reaches a zero reading at which time valve 1 is closed. The vacuum-pressure regulator (E) is then adjusted to zero ΔP on the manometer (F) and valve 3 is opened. A small ΔP is applied to the sample until the interface in the small bore capillary tube is near the middle of its length, at which time the vacuum-pressure regulator (E) is adjusted to keep the interface stationary. With valves 3 and 4 closed and valves 1 and 2 open, a small ΔP is applied to the burette. The value of the negative pressure applied will depend upon the magnitude of the bubbling pressure of the sample. A negative pressure of 2 or 3 cm of H_2O may be required for undisturbed samples while 5 cm or more may be used for fine textured disturbed samples. At this point, the



movement of the interface in the horizontal burette is used as an indicator of equilibrium. Equilibrium is attained very quickly when the sample is near complete saturation. For each additional negative pressure applied to the sample, the equilibrium burette and manometer readings are recorded.

When the bubbling pressure of the sample has been exceeded as indicated by a relatively large change in saturation for a small change in negative pressure, valves 1 and 2 may be closed at any particular volume reading on the burette. At the same time valves 3 and 4 are opened and the vacuum pressure regulator (E) is adjusted so that the interface in the small capillary tube does not appreciably move. The pressure is continually adjusted until no movement in the interface is detected over a period of perhaps five minutes.

At this time, the pressure of the liquid in the soil sample is nearly in equilibrium with the pressure applied to the interface of the capillary tube. To determine if complete equilibrium has been attained, valves 3 and 4 are closed and since 1 and 2 are already closed, this connects the soil sample to the differential pressure transducer. The transducer is sensitive to small pressure differences and final pressure adjustments may be made to obtain the equilibrium pressure reading. The transducer is used only to determine true equilibrium.

Additional desaturations are made by opening valves 1 and 2, closing valve 3, and increasing the negative pressure on manometer (F) until a predetermined volume has been extracted from the sample. The equilibrium pressure is obtained again by use of the small bore capillary tube and the differential pressure transducer. This procedure is repeated until sufficient data are obtained to define the curve or until the change in

saturation is small compared to changes in pressure. The final data point of capillary pressure may be as high as 0.4-0.5 mb.

After the final equilibrium pressure measurement has been made the imbibition curve is determined by keeping valves 1 and 2 permanently closed. A small volume of liquid is applied to the soil surface of the sample with valve 3 closed. The negative pressure is reduced and valve 3 is opened. The negative pressure is adjusted to maintain the interface in the small bore capillary tube at its null position. Final equilibrium pressure is obtained through the use of the differential pressure transducer as described above.

Additional increments of water are added and equilibrium pressure measurements are determined until zero capillary pressure is reached. The sum of the liquid increments added must equal the volume extracted on the drainage cycle.

BIBLIOGRAPHY

1. Ahuja, L. R. A Numerical and Similarity Analysis of Infiltration into Crusted Soils. *Water Resour. Res.* 9(4):987-994. 1973.
2. Braester, Carol. Moisture Variation at the Soil Surface and the Advance of the Wetting Front During Infiltration of Constant Flux. *Water Resour. Res.* 9(3):687-694. 1973.
3. Brooks, R. H. and A. T. Corey. Hydraulic Properties of Porous Media. Hydrology Paper No. 3. Colorado State University. 1966.
4. Brooks, R. H. and A. T. Corey. Properties of Porous Media Affecting Fluid Flow. *Jour. Irrigation and Drain. Div., Proceedings ASCE.* 92(IR2). 1966.
5. Brutsaert, Wilfried. A Solution for Vertical Infiltration into a Dry Porous Medium. *Water Resources Research.* 4(5):1031-1038. October 1968.
6. Colonna, J., F. Brissaud, and J. L. Millet. Evaluation of Capillarity and Relative Permeability Hysteresis. *Soc. Petroleum Engr. Jour.* pp. 28-38. February 1972.
7. Corey, G. L., A. T. Corey, and R. H. Brooks. Similitude for Non-Steady Drainage of Partially Saturated Soils. Hydrology Paper No. 9, Colorado State University. 1965.
8. Freeze, R. Allan. Three-Dimensional, Transient, Saturated-Unsaturated Flow in a Groundwater Basin. *Journal of Water Resources Research.* 7(2):347-366.
9. Jeppson, Roland W. Relationships of Infiltration Characteristics to Parameters Describing the Hydraulic Properties of Soils. Utah State University. PRWG-59C-7. 1972.
10. Land, Carlon S. Calculation of Imbibition Relative Permeability for Two and Three Phase Flow from Rock Properties. *Soc. Petroleum Engr. Jour.* pp 149-156. June 1968.
11. Lin, Shing Shong, Eugene W. Rochester, and Ronald E. Hermanson. Soil Moisture Profile Under Steady Infiltration. *J. Agric. Engr. Res.* (18). pp. 179-187. 1973.
12. Mein, Russel G. and Curtis L. Larson. Modeling Infiltration During a Steady Rain. *Water Resour. Res.* 9(2):384-394. 1973.
13. Mualem, Yechezkel. Modified Approach to Capillary Hysteresis Based on a Similarity Hypothesis. *Water Resour. Res.* 9(4):1324-1331. 1973.

14. Parlange, Jean-Yves. Comment on 'Absorption of Water by a Soil From a Circular Cylindrical Source', by R. Singh. *Water Resour. Res.* 9(4): 1098-1100. 1973.
15. Philip, J. R. Absorption and Infiltration in Two and Three Dimensional Systems. *Proc. UNESCO-Netherlands Symposium Water in the Unsaturated Zone*, Wageningen, The Netherlands. 1966.
16. Singh, R. Absorption of Water by a Soil From a Circular Cylindrical Source. *Water Resour. Res.* (8):1581-1589. 1972.
17. Singh, R. and J. B. Franzini. Unsteady Flow in Unsaturated Soils From a Cylindrical Source of Finite Radius. *J. Geophys. Res.* 72:1207-1215. 1967.
18. Skaggs, R. W., L. E. Huggins, E. J. Monke, and G. R. Foster. Experimental Evaluation of Infiltration Equations, *Transactions ASAE.* 12(6). 1969.
19. Ames, W. F. *Nonlinear Partial Differential Equations in Engineering.* Academic Press. 1965.
20. Saul'yev, V. K. Translated by G. J. Tee. *Integration of Equations of Parabolic Type by the Method of Nets.* The Macmillan Company, New York. 1964.